

Influence of lattice effects on the electron-positron interaction in metals

H. Sormann

Institut für Kernphysik, Technische Universität Graz, Petersgasse 16, A-8010 Graz, Austria

(Received 3 October 1995; revised manuscript received 8 February 1996)

We describe the influence of the crystal lattice on the enhancement of the electron-positron annihilation rate in metals by the use of an alternative version of the Bloch-modified ladder (BML) theory, which we call the *optimized* BML approximation. This approach to the problem of positrons interacting with an inhomogeneous electron gas can be reliably applied to metals with high and medium valence electron density, especially to transition metals, but is less efficient for metals with low electron densities such as, e.g., alkali metals. It enables us to describe the role of lattice effects in an approximative but nevertheless physically reasonable way. The paper offers (i) an extensive presentation of the theory and (ii) a summary of momentum-dependent enhancement results obtained for a series of simple and *d*-band metals (Al, Cu, Pd, Mn, and V) both for the central momentum region and for near umklapp regions. These BML enhancement factors are compared with corresponding results of the local-density approximation and with enhancement factors extracted from two-dimensional angular correlation experiments. The main result of this paper is that we are able to demonstrate that for all metals and for all regions of the momentum space investigated, the lattice effects on the electron-positron enhancement are significant and therefore should not be neglected in theoretical work. [S0163-1829(96)02131-5]

I. INTRODUCTION

For a reliable interpretation of positron annihilation experiments (e.g., lifetime or angular correlation measurements) in metallic systems, an understanding of the Coulombic electron-positron (*e-p*) interaction and the *enhancement* of the annihilation rate due to this interaction is of vital importance. Usually, theoretical investigations about the *e-p* interaction in metals start with the corresponding *jellium* problem, i.e., with the study of the behavior of electron-positron pairs in a *homogeneous* electron gas. A successful calculation of the momentum-dependent enhancement of the electron density at positron position in jellium was done by Kahana¹ by a summation of ladder diagrams of the electron-positron two-particle Green's function. There is a general agreement that this approximative description of a typical many-body problem by electron-positron pairs embedded in an electron gas is reasonable as long as the electron density within the metal is not too low and the probability of the creation of *e-p* bound states is small. Later refinements of Kahana's theory are due to Boroński *et al.*² and to Rubaszek and Stachowiak,³ who presented a fully self-consistent solution of the Kahana equation. Other independent theories on positron enhancement in jellium elaborated by several authors can be found in the literature (see, e.g., the review article by Stachowiak and Rubaszek⁴ and the references therein). Due to all these efforts, we can say that the physics of positrons annihilating in a homogeneous electron gas is essentially well understood.

However, this is by no means the case for the *e-p* interaction within an *inhomogeneous* electron gas ("beyond jellium") where one has to face the problem that both the electrons and positrons are submitted to an external potential that is periodic with respect to the lattice of the metal ions. This lattice potential causes two important features in the momentum density of annihilation pairs (MDAP) of electrons and

positrons, namely, at first, the appearance of high-momentum (umklapp) components (HMC's) whose intensity is relatively small for *sp*-like valence electrons but may be considerably large for *d*-like or *f*-like electrons in transition or noble metals or for tightly bound core electrons. Second, there is some evidence that both the strength and the momentum dependence of the enhancement for *d*-like and *f*-like electrons is different from the results of the Kahana theory. Both effects can be empirically described by using Kahana-like but energy-dependent enhancement factors (according to an idea of Sob^{5,6} and, independently, Mijnaerends and Singru⁷) and by state-dependent enhancement factors with different coefficients for *sp*-like and *d*-like electron states.^{8,9} These ideas were successfully used in many other investigations; see, e.g., Refs. 10–15.

An important aspect in the theory of the electron-positron interaction was the use of *local* enhancement factors. This idea goes back to papers by Bonderup *et al.*¹⁶ and Chakraborty¹⁷ and was further developed by Daniuk *et al.*^{18,19} and similarly by Jarlborg and Singh.²⁰ All these efforts led to a local-density approximation (LDA) for the calculation of the *e-p* enhancement in condensed matter. The basic principles of the LDA are given in Sec. III of this paper; for more detailed information see the recent review article by Sob²¹ and the references therein.

During the past decade, different versions of the LDA were successfully used for investigations on positron annihilation in various materials such as simple metals (alkali metals, magnesium),^{22–25} *3d* and *4d* metals,^{18–20,22,26,27} alloys,²⁸ and high- T_c superconductors.^{29–31} Systematic investigations on electron-positron enhancement factors in metals based on the LDA may be found in Refs. 32–37 and their mutual comparison with respect to the agreement with experiment in Ref. 38; a thorough theoretical analysis of the LDA for positrons is performed in Ref. 39.

Extensively discussed in many of these LDA investiga-

tions is the question whether the high-momentum components of the MDAP are *less* or *more* enhanced by e - p interaction effects than the components of the central-momentum region. In the literature, such effects are called *deenhancement* or *overenhancement* of the annihilation rate, respectively. An exact definition of these effects is given at the beginning of Sec. VIII D 2. A deenhancement effect was predicted by Fujiwara *et al.*⁴⁰ and was studied in some early papers by Hede and Carbotte,⁴¹ Sormann *et al.*^{42,43} and Sob.^{5,9,44-46} Over the past years, the possibility of the controversial overenhancement effect of HMC's has been studied in Refs. 23 24, and 27.

A second important feature of the e - p annihilation in metals, namely, the decrease of the d -electron enhancement factor with increasing momentum, for which there is some experimental evidence,^{10,11} was also observed in LDA studies.^{20,26} Both this topic and the question of deenhancement or overenhancement of HMC annihilation rates in metals will be discussed in Sec. VIII of this paper.

Despite the impressive results of the LDA, this approach is incomplete in the following sense: it does not explicitly take into account the influence of the crystal lattice on the electron-positron interaction. It is clear that all Coulombic interactions between electrons and positrons can be considered as scattering processes where the particles are scattered out of their occupied states. As we shall show in Sec. II from a more mathematical point of view, we have to deal with two quite different types of scattering processes, namely, (i) between the electron and positron that constitute the annihilating pair and (ii) between all other electrons that react to the existence of the disturbing positron by a polarization of the electron gas. In both cases, unoccupied electron and positron Bloch states appear that are not included in the local-density approach.

The influence of these lattice effects on the positron annihilation in metals is the main topic of the present paper, where we focus our attention on the interaction of thermalized positrons with *itinerant* electrons, i.e., with sp -like and nearly free valence electrons, and with d -like electrons in transition and noble metals, which also have an itinerant character but are more tightly bound to the atomic nuclei than the sp electrons. The annihilation of positrons with core electrons and of positrons trapped in defects of the lattice are not treated in the present investigation.

An inclusion of lattice effects in the enhancement theory of metals is, in principle, possible by an application of Kahana's theory to the nonjellium case, i.e., to an inhomogeneous electron gas. Such a procedure was proposed by Carbotte⁴⁷ and was used for an approximative calculation of the enhancement for core electrons.⁴⁸ This approach [for which the present author proposed the name *Bloch-modified ladder* (BML) theory] is based on a numerical solution of the Bethe-Goldstone equation for the inhomogeneous electron gas. The mathematical background of the BML is given in detail in Refs. 47 and 49 and is briefly reviewed in Secs. IV and V of this paper.

Unfortunately, Carbotte's approach is much too complicated to be used for a calculation of the enhancement of the annihilation rate of positrons interacting with itinerant metal electrons. Therefore, based on Carbotte's work, Sormann and Puff⁴³ published a lattice-modified Kahana theory, where

in the ladder expansion of the e - p Green's function the "Bloch character" of the interacting electrons and positrons is at least partly taken into account. Because of the approximations included in this approach, which is described in detail in Refs. 43 and 50 and in Sec. VI, it was called the *quasifree* (QF) BML theory. An application of the QF BML theory to the enhancement of the HMC's in alkali metals⁴³ gave a qualitative indication of a more or less pronounced deenhancement effect. At least for lithium, the QF BML results within the (110) umklapp region⁵⁰ led to significantly better agreement between experiment⁵¹ and theory. Additionally, the QF BML theory also yields the typical non-Kahana-like momentum dependence of enhancement factors of d -electrons in metals, as it was shown for the noble metals copper and silver⁵² and the transition metals nickel and iron.⁵³

Over the past years, some efforts were made to improve the ladder approach for the inhomogeneous electron gas by a physically more realistic description of the electron and positron scattering states. We mention here in particular the work of Boroński, Jarlberg, and co-workers,⁵⁴⁻⁵⁶ which is based on the approximative evaluation of the Bethe-Goldstone equation using single-particle Bloch functions for the electrons and parametrized positron wave functions. The effective e - p interaction potential is given as a local function dependent on the position of the positron. From this point of view, this work of Boroński and Jarlberg represents a combination of the LDA with Bloch state scattering effects. We shall return to this approach in Secs. VII A and VIII E.

In 1992, the present author started to develop the QF BML approach with the aim of a more efficient inclusion of lattice effects into the theory. Apart from some preliminary reports,⁵⁷⁻⁶⁰ this paper offers an extensive presentation of the result of those efforts, the so-called *optimized* BML (OBML) theory. Mathematical and numerical details of this approach, including a discussion about its applicability, are given in Sec. VII. It turns out that the OBML theory is very efficient for all metals with high and medium valence electron density (such as, e.g., aluminum, copper, and transition metals), but is less qualified for metals with low electron densities such as, e.g., alkali metals. In Sec. VIII, after some general remarks on the e - p interaction potential, we present a comparison between OBML and LDA enhancement results for the simple metal Al and the d -band metals Cu, Pd, Mn, and V for both the central momentum region and near HMC regions. A confrontation of OBML and LDA results with enhancement factors extracted from two-dimensional (2D) angular correlation of positron annihilation radiation (ACPAR) experiments is also given in Sec. VIII, followed by a conclusion of this paper in Sec. IX.

II. BASIC NOTIONS AND DEFINITIONS

All theoretical investigations on the electron-positron interaction in metals, especially if one deals with itinerant electrons as we do in this paper, are based on the well-known formula for the two-particle momentum density of annihilation pairs⁶¹

$$\rho_{2\gamma}(\mathbf{p}) = (-i)^2 \int_{\Omega} d^3x d^3y \exp[-i\mathbf{p} \cdot (\mathbf{x} - \mathbf{y})] \times G_{ep}(\mathbf{x}t, \mathbf{x}t; \mathbf{y}t^+, \mathbf{y}t^+), \quad (1)$$

where $\hbar\mathbf{p}$ is the photon-pair momentum, Ω is the volume of the crystal, and G_{ep} represents the zero-temperature electron-positron Green's function. The arguments of this function describe the propagation of an electron-positron pair from space point \mathbf{x} to space point \mathbf{y} during the (infinitesimally small) time difference $t^+ - t$. The corresponding momentum-dependent rate $R_{2\gamma}(\mathbf{p})$ for a two-photon (2γ) annihilation is given by

$$R_{2\gamma}(\mathbf{p}) = 2 \frac{r_0^2 \pi c}{\Omega} \rho_{2\gamma}(\mathbf{p}), \quad (2)$$

with r_0 and c the classical electron radius and the velocity of light, respectively, and the factor 2 accounting for the spin degeneracy.

Following Kahana¹ and his enhancement theory for the homogeneous electron gas, G_{ep} can be approximated by the integral equation

$$G_{ep}^L(x, x'; y, y') = G_e(x, y) G_p(x', y') + \frac{i}{\hbar} \int dz dz' G_e(x, z) G_p(x', z') V^{ep}(z, z') \times G_{ep}^L(z, z'; y, y'), \quad (3)$$

with $x \equiv \mathbf{x}t_x$, $y \equiv \mathbf{y}t_y$, $x' \equiv \mathbf{x}'t_{x'}$, $y' \equiv \mathbf{y}'t_{y'}$, $z \equiv \mathbf{z}t_z$, and $z' \equiv \mathbf{z}'t_{z'}$. G_e and G_p are the single-particle Green's functions for an electron and a positron, respectively, and V^{ep} describes the effective interaction potential between the two fermions. The superscript L in Eq. (3) stands for *ladder* approximation or *ladder* expansion because of the ladder form of the corresponding Feynman diagrams. The single-particle Green's function for a noninteracting electron propagating within a lattice-periodic potential is given by the expression⁶²

$$G_e(\mathbf{x}t_x, \mathbf{y}t_y) = \lim_{\eta \rightarrow 0^+} \frac{1}{2\pi} \int_{-\infty}^{+\infty} d\omega e^{-i\omega(t_x - t_y)} \sum_{n, \mathbf{k}} \psi_{n\mathbf{k}}(\mathbf{x}) \psi_{n\mathbf{k}}^*(\mathbf{y}) \times \left[\frac{\Theta(E_F - E_{n\mathbf{k}})}{\omega - E_{n\mathbf{k}}/\hbar - i\eta} + \frac{\Theta(E_{n\mathbf{k}} - E_F)}{\omega - E_{n\mathbf{k}}/\hbar + i\eta} \right], \quad (4)$$

where $\psi_{n\mathbf{k}}$ means an electron wave function with the band index n and the Bloch vector \mathbf{k} within the first Brillouin zone (BZ). $E_{n\mathbf{k}}$ is the corresponding eigenenergy, and the step function Θ accounts for the Fermi-Dirac distribution of occupied fermions at zero temperature. Similarly, the single-particle Green's function for a positron has the form⁶²

$$G_p(\mathbf{x}t_x, \mathbf{y}t_y) = \lim_{\eta \rightarrow 0^+} \frac{1}{2\pi} \int_{-\infty}^{+\infty} d\omega e^{-i\omega(t_x - t_y)} \sum_{n, \mathbf{k}} \varphi_{n\mathbf{k}}(\mathbf{x}) \varphi_{n\mathbf{k}}^*(\mathbf{y}) \times \left[\frac{\delta_{n\mathbf{k}, 10}}{\omega - E_{n\mathbf{k}}^+/\hbar - i\eta} + \frac{1 - \delta_{n\mathbf{k}, 10}}{\omega - E_{n\mathbf{k}}^+/\hbar + i\eta} \right], \quad (5)$$

with the positron Bloch states $\varphi_{n\mathbf{k}}$ and the corresponding eigenenergies $E_{n\mathbf{k}}^+$. Due to the fact that in a positron annihilation experiment there is usually only one positron in the sample, the only occupied positron state will be situated at the bottom of the lowest band ($n=1$) at the Γ point ($\mathbf{k}=\mathbf{0}$). Taking this into account, in Eq. (5), the step function of Eq. (4) has to be replaced by the Kronecker delta.

The $\psi_{n\mathbf{k}}$ and $\varphi_{n\mathbf{k}}$ are solutions of the single-particle Schrödinger-like equations

$$\left[-\frac{\hbar^2}{2m} \Delta + V_c^-(\mathbf{r}) + V_{xc}^-(\mathbf{r}) \right] \psi_{n\mathbf{k}}(\mathbf{r}) = E_{n\mathbf{k}} \psi_{n\mathbf{k}}(\mathbf{r}), \quad (6)$$

$$\left[-\frac{\hbar^2}{2m} \Delta + V_c^+(\mathbf{r}) + V_{\text{corr}}^{+-}(\mathbf{r}) \right] \varphi_{n\mathbf{k}}(\mathbf{r}) = E_{n\mathbf{k}}^+ \varphi_{n\mathbf{k}}(\mathbf{r}). \quad (7)$$

In these equations, V_c^\pm means the Coulombic potential energy of the particle due to the (rigid) lattice of the atomic ions and the Hartree potential, V_{xc}^- represents the LDA of the exchange and the (static) correlation of the electron with the other electrons, and V_{corr}^{+-} in Eq. (7) is the single-particle electron-positron correlation potential, also in the LDA, eventually in a parametrized form as it has been published by Boronksi and Nieminen.⁶³ This potential must be distinguished from the two-particle e - p interaction potential V^{ep} , which appears in Eq. (3) for the electron-positron Green's function. From the point of view of a perturbation expansion of G_{ep} , V_{corr}^{+-} represents a self-energy insertion into the positron Green's function, whereas V^{ep} describes the two-particle interaction of the annihilating electron-positron pair. Concerning the enhancement, this potential is usually much more important than the self-energy effect. For this reason, the V_{corr}^{+-} in Eq. (7) is neglected in many theoretical investigations and also in the work presented. But it should be emphasized that this neglect might not be justified in each case. For example, as we learned from a paper of Daniuk, Šob, and Rubaszek,³³ for the core annihilation, the effect of V_{corr}^{+-} might be significant.

According to Eqs. (1)–(5), all lattice effects result from the fact that, in crystalline systems, the electron and positron Green's functions (4) and (5) have to be based on Bloch waves. Therefore, we have to deal with two principally different influences of the crystal lattice on the electron-positron Green's function G_{ep} and, consequently, on the MDAP: (i) the lattice effect on the scattering processes between the annihilating electrons and positrons is included in the single-particle Green's functions G_e and G_p that appear explicitly in the integral equation (3) and (ii) the lattice effect on the polarization of the electron gas is included in the electron Green's functions G_e that implicitly appear in the interaction potential V^{ep} in Eq. (3); more details about this subject are given in Sec. V. Henceforth in this paper, the compact terms “lattice effect on the e - p scattering” and “lattice effect on the polarization” will be used in the sense described above.

Taking into account only the first term of the ladder expansion (3), i.e., the term of zeroth order with respect to V^{ep} , and also neglecting the effect of the correlation potential V_{corr}^{+-} in the single-particle Schrödinger equation (7), one gets the electron-positron Green's function according to the

independent-particle model (IPM), which is simply a product of the electron and positron single-particle Green's functions

$$G_{ep}^{\text{IPM}}(x, x'; y, y') = G_e(x, y) G_p(x', y').$$

Inserting this approximation into Eq. (1) and using the Green's functions (4) and (5), one obtains the well-known formula for the MDAP in the IPM, namely,

$$\rho_{2\gamma}^{\text{IPM}}(\mathbf{p}) = \sum_{n, \mathbf{q}} \Theta(E_F - E_{n\mathbf{q}}) \delta_{\mathbf{p} - \mathbf{K} - \mathbf{q}, \mathbf{0}} \left| \frac{\Omega}{\Omega_0} \int_{\Omega_0} d^3 r \right. \\ \left. \times \exp(-i\mathbf{p} \cdot \mathbf{r}) \psi_{n\mathbf{q}}(\mathbf{r}) \varphi_{10}(\mathbf{r}) \right|^2, \quad (8)$$

where \mathbf{K} denotes a reciprocal-lattice vector such that $\mathbf{p} - \mathbf{K}$ lies in the first BZ and φ_{10} means the only occupied bottom state of the positron. \mathbf{q} is also a vector of the first BZ. The spatial integral is over the volume of a unit cell of the crystal (Ω_0) and the unusual factor Ω/Ω_0 before the integral comes from the fact that, in this paper, all electron and positron Bloch states are consequently normalized with respect to the crystal volume Ω . For practical reasons, it is advantageous to write the vector \mathbf{p} as a sum of a vector \mathbf{k} that is an element of the first BZ and a reciprocal-lattice vector \mathbf{G} . Henceforth, we call \mathbf{k} a *reduced* vector and \mathbf{p} an *extended* vector of the momentum space. Then the above expression gets the relatively simple form

$$\rho_{2\gamma}^{\text{IPM}}(\mathbf{k} + \mathbf{G}) = \sum_n \Theta(E_F - E_{n\mathbf{k}}) \left| \frac{\Omega}{\Omega_0} \int_{\Omega_0} d^3 r \right. \\ \left. \times \exp[-i(\mathbf{k} + \mathbf{G}) \cdot \mathbf{r}] \psi_{n\mathbf{k}}(\mathbf{r}) \varphi_{10}(\mathbf{r}) \right|^2, \quad (9)$$

where $\mathbf{G} = \mathbf{0}$ corresponds to photon-pair momenta within the first BZ, i.e., to the low-momentum component (LMC) of the MDAP, whereas $\mathbf{G} \neq \mathbf{0}$ describes the high-momentum component (HMC) of the MDAP centered around the vector \mathbf{G} .

III. THE LOCAL-DENSITY APPROXIMATION

As we already mentioned in the Introduction, in this section, we describe only some of the key points of the LDA. It is based on a MDAP formula that is very similar to the IPM expression Eq. (9) but includes electron-positron correlations by the insertion of a *local* pair-correlation function $g(\mathbf{r}; n\mathbf{k})$, which is an electron-state-dependent function of the electron density at a given point \mathbf{r} and describes the local enhancement of the electron-positron interaction:

$$\rho_{2\gamma}^{\text{LDA}}(\mathbf{k} + \mathbf{G}) = \sum_n \Theta(E_F - E_{n\mathbf{k}}) \\ \times \left| \frac{\Omega}{\Omega_0} \int_{\Omega_0} d^3 r \exp[-i(\mathbf{k} + \mathbf{G}) \cdot \mathbf{r}] \right. \\ \left. \times \sqrt{g(\mathbf{r}; n\mathbf{k})} \psi_{n\mathbf{k}}(\mathbf{r}) \varphi_{10}(\mathbf{r}) \right|^2. \quad (10)$$

For our comparative calculations between the LDA and the BML approximation presented in Sec. VIII, we decided to

use the formulation of Daniuk *et al.*,^{18,19,33} where g is taken from the enhancement theory of the homogeneous electron gas

$$g(\mathbf{r}; n\mathbf{k}) = \epsilon_{\text{hom}}[r_s(\mathbf{r}); X_{n\mathbf{k}}]. \quad (11)$$

$r_s(\mathbf{r}) = [4\pi n(\mathbf{r})/3]^{-1/3}$ is the local-density parameter [$n(\mathbf{r})$ being the total local electron density] and

$$X_{n\mathbf{k}} = \sqrt{(E_{n\mathbf{k}} - E_{10})/(E_F - E_{10})}, \quad (12)$$

where $E_{n\mathbf{k}}$ and E_F mean the energy of the initial electronic state $|n\mathbf{k}\rangle$ and the Fermi energy, respectively, and E_{10} is the bottom energy of the electron conduction bands. This energy-dependent enhancement for individual states was proposed by Šob^{5,6} and independently by Mijnrends and Singru.⁷

It must be noted here that Eq. (12) does not correspond to the original LDA formulation by Daniuk *et al.*,^{18,19} where the momentum-dependent part of g was also considered a local function, namely,

$$X_{n\mathbf{k}}(\mathbf{r}) = \sqrt{[E_{n\mathbf{k}} - V^-(\mathbf{r})]/[E_F - V^-(\mathbf{r})]},$$

where $V^-(\mathbf{r}) = V_c^-(\mathbf{r}) + V_{\text{xc}}^-(\mathbf{r})$ is the crystal potential energy of a Bloch electron according to Eq. (6). There is some evidence that a nonlocal momentum factor as defined by Eq. (12) is more appropriate from the physical point of view,^{33,64} but the discussion about this detail of the LDA approach is not yet finished. In this connection, it should be expressed that it is one of the advantages of the BML theory described in the following sections that, in contrast to the LDA, no assumptions about the momentum or energy dependence of the local enhancement is necessary. It should also be mentioned here that some more basic objections concerning the LDA were recently formulated by Stachowiak.⁶⁵

IV. THE BLOCH-MODIFIED LADDER THEORY

The attempt of an application of the Kahana theory [Eqs. (1) and (3)] to the inhomogeneous electron gas was presented by Carbotte.⁴⁷ In principle, this procedure is straightforward by inserting the electron and positron Green's functions based on Bloch states [Eqs. (5) and (6)] into Kahana's integral equation (3) and the MDAP formula (1). For this mathematical treatment, it is useful to expand the electron and positron Bloch functions into plane waves, namely,

$$\psi_{n\mathbf{k}}(\mathbf{r}) = \frac{1}{\sqrt{\Omega}} \sum_{\mathbf{K}} a_{n\mathbf{k}}(\mathbf{K}) \exp[i(\mathbf{k} + \mathbf{K}) \cdot \mathbf{r}] \quad (13)$$

and

$$\varphi_{n\mathbf{k}}(\mathbf{r}) = \frac{1}{\sqrt{\Omega}} \sum_{\mathbf{K}} b_{n\mathbf{k}}(\mathbf{K}) \exp[i(\mathbf{k} + \mathbf{K}) \cdot \mathbf{r}], \quad (14)$$

respectively, with \mathbf{K} being a reciprocal-lattice vector and $a_{n\mathbf{k}}(\mathbf{K})$ and $b_{n\mathbf{k}}(\mathbf{K})$ the corresponding Fourier coefficients. In the following, we take advantage of the fact that the $a_{n\mathbf{k}}$ and $b_{n\mathbf{k}}$ are real numbers for all Bravais lattices and some other high-symmetrical lattices such as hcp. With the use of the above expansions, one gets, after a rather lengthy and

tedious calculation,⁴⁹ which cannot be presented here in detail, the basic formulas of the so-called exact *Bloch-modified ladder* theory

$$\begin{aligned} \rho_{2\gamma}^{\text{BML}}(\mathbf{k}+\mathbf{G}) &= \sum_n \Theta(E_F - E_{n\mathbf{k}}) \left[\sum_{\mathbf{K}} a_{n\mathbf{k}}(\mathbf{K}) b_{10}(\mathbf{G}-\mathbf{K}) \right. \\ &+ \frac{1}{\Omega} \sum_i \sum_{\mathbf{k}'} \Theta(E_{i\mathbf{k}'} - E_F) \sum_j (E_{n\mathbf{k}} - E_{i\mathbf{k}'}) \\ &+ E_{10}^+ - E_{j\mathbf{q}}^+)^{-1} \chi_{i,j;\mathbf{G}}^{\text{BML}}(\mathbf{k}') \\ &\times \sum_{\mathbf{G}_1} \sum_{\mathbf{G}_2} V_{\mathbf{G}_1, \mathbf{G}_2}^{ep}(\mathbf{q}) \left[\sum_{\mathbf{K}_2} a_{n\mathbf{k}}(\mathbf{K}_2) \right. \\ &\times a_{i\mathbf{k}'}(\mathbf{K}_2 - \mathbf{G}_1 + \mathbf{L}) \left. \right] \\ &\times \left. \left[\sum_{\mathbf{K}_3} b_{10}(\mathbf{K}_3) b_{j\mathbf{q}}(\mathbf{K}_3 + \mathbf{G}_2) \right] \right\}^2, \end{aligned} \quad (15)$$

including the *Bloch-modified Bethe-Goldstone amplitude* χ^{BML}

$$\begin{aligned} \chi_{i,j;\mathbf{G}}^{\text{BML}}(\mathbf{k}') &= \sum_{\mathbf{K}_1} a_{i\mathbf{k}'}(\mathbf{K}_1) b_{j\mathbf{q}}(\mathbf{G} - \mathbf{K}_1 + \mathbf{L}) \\ &+ \frac{1}{\Omega} \sum_s \sum_{\mathbf{k}''} \Theta(E_{s\mathbf{k}''} - E_F) \\ &\times \sum_t (E_{n\mathbf{k}} - E_{s\mathbf{k}''} + E_{10}^+ - E_{t\mathbf{q}'}^+)^{-1} \\ &\times \chi_{s,t;\mathbf{G}}^{\text{BML}}(\mathbf{k}'') \sum_{\mathbf{G}', \mathbf{G}''} V_{\mathbf{G}', \mathbf{G}''}^{ep}(\mathbf{q}'') \\ &\times \left[\sum_{\mathbf{K}_2} a_{i\mathbf{k}'}(\mathbf{K}_2) a_{s\mathbf{k}''}(\mathbf{K}_2 - \mathbf{G}' + \mathbf{L}'') \right] \\ &\times \left[\sum_{\mathbf{K}_3} b_{j\mathbf{q}}(\mathbf{K}_3) b_{t\mathbf{q}'}(\mathbf{K}_3 + \mathbf{G}'' - \mathbf{L} + \mathbf{L}' - \mathbf{L}'') \right]. \end{aligned} \quad (16)$$

In Eqs. (15) and (16), the $a_{n\mathbf{k}}$ mean the Fourier coefficients of the occupied electron states and the $E_{n\mathbf{k}}$ are the corresponding energies. The only occupied positron state is represented by the Fourier coefficients $b_{10}(\mathbf{K})$ and the corresponding energy E_{10}^+ . All other Fourier coefficients and energies with the band indices i, j, s, t , etc., and the reduced Bloch vectors $\mathbf{k}', \mathbf{q}, \mathbf{k}'', \mathbf{q}'$, etc., belong to unoccupied electron and positron (scattering) states. The reciprocal-lattice vectors \mathbf{L}, \mathbf{L}' , and \mathbf{L}'' in Eqs. (15) and (16) are defined by the conditions that the vectors $\mathbf{q} = \mathbf{k} - \mathbf{k}' - \mathbf{L}$, $\mathbf{q}' = \mathbf{k} - \mathbf{k}'' - \mathbf{L}'$, and $\mathbf{q}'' = \mathbf{k}' - \mathbf{k}'' - \mathbf{L}''$ must also belong to the first BZ.

V. THE EFFECTIVE ELECTRON-POSITRON INTERACTION

Until now, we did not say anything about the effective electron-positron interaction potential V^{ep} that appears in

Eqs. (15) and (16). The theory of fermion-fermion interactions in spatially inhomogeneous systems is extensively discussed in the literature (see, e.g., Refs. 66–68 and references therein) and we shall give here only a short summary of this subject.

Due to the spatial inhomogeneity of the electron gas, the two-particle interaction potential between the electron and positron can be expressed as a function $V^{ep}(\mathbf{x}, \mathbf{y}; t_x - t_y)$, which depends explicitly on the positions of both interacting particles and not simply on the relative coordinate $\mathbf{x} - \mathbf{y}$. Such a function can be Fourier transformed as

$$\begin{aligned} V^{ep}(\mathbf{x}, \mathbf{y}; t_x - t_y) &= \frac{1}{2\pi\Omega} \sum_{\mathbf{p}_1} \sum_{\mathbf{p}_2} e^{i\mathbf{p}_1 \cdot \mathbf{x}} e^{-i\mathbf{p}_2 \cdot \mathbf{y}} \\ &\times \int_{-\infty}^{+\infty} d\omega e^{-i\omega(t_x - t_y)} V^{ep}(\mathbf{p}_1, \mathbf{p}_2; \omega), \end{aligned} \quad (17)$$

where \mathbf{p}_1 and \mathbf{p}_2 are vectors of the extended momentum space and $V^{ep}(\mathbf{p}_1, \mathbf{p}_2; \omega)$ is the corresponding Fourier coefficient. With the vector sums

$$\mathbf{p}_1 = \mathbf{q}_1 + \mathbf{G}_1, \quad \mathbf{p}_2 = \mathbf{q}_2 + \mathbf{G}_2,$$

where \mathbf{q}_1 and \mathbf{q}_2 are vectors of the first BZ and \mathbf{G}_1 and \mathbf{G}_2 are reciprocal-lattice vectors, Eq. (17) may be written in the form

$$\begin{aligned} V^{ep}(\mathbf{x}, \mathbf{y}; t_x - t_y) &= \frac{1}{2\pi\Omega} \sum_{\mathbf{q}_1} \sum_{\mathbf{q}_2} \sum_{\mathbf{G}_1} \sum_{\mathbf{G}_2} e^{i(\mathbf{q}_1 + \mathbf{G}_1) \cdot \mathbf{x}} e^{-i(\mathbf{q}_2 + \mathbf{G}_2) \cdot \mathbf{y}} \\ &\times \int_{-\infty}^{+\infty} d\omega e^{-i\omega(t_x - t_y)} V^{ep}(\mathbf{q}_1 + \mathbf{G}_1, \mathbf{q}_2 + \mathbf{G}_2; \omega). \end{aligned}$$

This function must have the same symmetry group as the crystal structure of the solid, with respect to both spatial arguments \mathbf{x} and \mathbf{y} . In particular, the condition

$$V^{ep}(\mathbf{x} + \mathbf{R}, \mathbf{y} + \mathbf{R}; t_x - t_y) = V^{ep}(\mathbf{x}, \mathbf{y}; t_x - t_y)$$

must be fulfilled for each lattice translation vector \mathbf{R} of the crystal. After a short calculation, this leads to

$$\mathbf{q}_1 = \mathbf{q}_2 = \mathbf{q}$$

and consequently to the expression

$$\begin{aligned} V^{ep}(\mathbf{x}, \mathbf{y}; t_x - t_y) &= \frac{1}{2\pi\Omega} \sum_{\mathbf{q}} e^{i\mathbf{q} \cdot (\mathbf{x} - \mathbf{y})} \sum_{\mathbf{G}_1} \sum_{\mathbf{G}_2} e^{i\mathbf{G}_1 \cdot \mathbf{x}} e^{-i\mathbf{G}_2 \cdot \mathbf{y}} \\ &\times \int_{-\infty}^{+\infty} d\omega e^{-i\omega(t_x - t_y)} \\ &\times V^{ep}(\mathbf{q} + \mathbf{G}_1, \mathbf{q} + \mathbf{G}_2; \omega). \end{aligned} \quad (18)$$

Due to the fact that \mathbf{G}_1 and \mathbf{G}_2 are discrete quantities, the Fourier transform of V^{ep} can be considered a matrix

$$V^{ep}(\mathbf{q} + \mathbf{G}_1, \mathbf{q} + \mathbf{G}_2; \omega) \equiv V_{\mathbf{G}_1, \mathbf{G}_2}^{ep}(\mathbf{q}; \omega). \quad (19)$$

For a system with infinitesimal translation invariance (e.g., for the jellium), the matrix simplifies substantially to a diag-

onal matrix, which means that all information about the spatial inhomogeneity (i.e., about local-field effects) of the e - p interaction potential is contained in the off-diagonal elements of $V_{\mathbf{G}_1, \mathbf{G}_2}^{ep}$.

Analogous to the theory of the homogeneous electron gas, the Fourier transform of the effective electron-positron interaction potential can be written as⁶⁶

$$V_{\mathbf{G}_1, \mathbf{G}_2}^{ep}(\mathbf{q}, \omega) = - \frac{4\pi e^2}{|\mathbf{q} + \mathbf{G}_1||\mathbf{q} + \mathbf{G}_2|} [\kappa(\mathbf{q}, \omega)]_{\mathbf{G}_1, \mathbf{G}_2}^{-1}, \quad (20)$$

with e as the electron charge and κ^{-1} as the inverse of the Hermitian dielectric matrix⁶⁷

$$\kappa_{\mathbf{G}_1, \mathbf{G}_2}(\mathbf{q}, \omega) = \delta_{\mathbf{G}_1, \mathbf{G}_2} - \frac{4\pi e^2}{|\mathbf{q} + \mathbf{G}_1||\mathbf{q} + \mathbf{G}_2|} P_{\mathbf{G}_1, \mathbf{G}_2}(\mathbf{q}, \omega), \quad (21)$$

where P represents the matrix of the Fourier transform of the polarizability of the electron gas, which is defined by an expression similar to Eq. (18), namely,

$$P(\mathbf{x}, \mathbf{y}; t_x - t_y) = \frac{1}{2\pi\Omega} \sum_{\mathbf{q}} e^{i\mathbf{q} \cdot (\mathbf{x} - \mathbf{y})} \sum_{\mathbf{G}_1} \sum_{\mathbf{G}_2} e^{i\mathbf{G}_1 \cdot \mathbf{x}} e^{-i\mathbf{G}_2 \cdot \mathbf{y}} \times \int_{-\infty}^{+\infty} d\omega e^{-i\omega(t_x - t_y)} P_{\mathbf{G}_1, \mathbf{G}_2}(\mathbf{q}, \omega). \quad (22)$$

The simplest approximation of P , the random-phase approximation (RPA), is, in real space, given by⁶⁹

$$P^{\text{RPA}}(\mathbf{x}, \mathbf{y}; t_x - t_y) = - \frac{2i}{\hbar} G_e(\mathbf{x}t_x, \mathbf{y}t_y) G_e(\mathbf{y}t_y, \mathbf{x}t_x). \quad (23)$$

If the electron Green's functions in this equation are based on Bloch waves [see Eq. (4)], we have to expect lattice effects on the polarization as they were defined in Sec. II. Combining Eqs. (4), (22), and (23) and using the Fourier expansion of the electron wave functions (13), we get the matrix elements $P_{\mathbf{G}_1, \mathbf{G}_2}(\mathbf{q}, \omega)$ in the RPA. If we neglect the dynamical aspects of the screening of the e - p interaction, as is frequently done in positron physics (see the discussion in Sec. VIII A), we obtain according to Adler and Wisner,⁶⁶ but in a somewhat different formulation,

$$P_{\mathbf{G}_1, \mathbf{G}_2}^{\text{RPA}}(\mathbf{q}, 0) \equiv P_{\mathbf{G}_1, \mathbf{G}_2}^{\text{RPA}}(\mathbf{q}) = - \frac{4}{\Omega} \sum_n \sum_{\mathbf{k}'} \Theta(E_F) - E_{n\mathbf{k}'} \sum_m \Theta(E_{m\mathbf{k}''} - E_F) \times (E_{m\mathbf{k}''} - E_{n\mathbf{k}'})^{-1} M_{n\mathbf{k}'; m\mathbf{k}''} \times (\mathbf{q}, \mathbf{G}_1) M_{n\mathbf{k}'; m\mathbf{k}''}(\mathbf{q}, \mathbf{G}_2), \quad (24)$$

with

$$M_{n\mathbf{k}'; m\mathbf{k}''}(\mathbf{q}, \mathbf{G}) = \sum_{\mathbf{K}} a_{n\mathbf{k}'}(\mathbf{K}) a_{m\mathbf{k}''}(\mathbf{K} - \mathbf{G} + \mathbf{L}). \quad (25)$$

In the above equations, Ω means the crystal volume and E_F is the Fermi energy of the electron gas. The quantities

$E_{n\mathbf{k}'}$ and $a_{n\mathbf{k}'}$ are the energies and the Fourier coefficients of the occupied electron states $|n\mathbf{k}'\rangle$; correspondingly, the $E_{m\mathbf{k}''}$ and $a_{m\mathbf{k}''}$ belong to the unoccupied electron states $|m\mathbf{k}''\rangle$. The vector \mathbf{k}'' and the reciprocal-lattice vector \mathbf{L} are defined by the condition that $\mathbf{k}'' \equiv \mathbf{k}' - \mathbf{q} - \mathbf{L}$ is an element of the first BZ, where both \mathbf{k}' and \mathbf{q} also belong to the first BZ.

It should be mentioned here that, in the literature, the dielectric and the polarizability matrices are usually denoted ϵ and χ , respectively. The unusual notations κ and P in this paper come from the fact that, in positron physics, the letters ϵ and χ are reserved for the enhancement factor and the Bethe-Goldstone amplitude.

VI. THE QUASIFREE BML APPROXIMATION

An uncompromising evaluation of the BML equations (15) and (16) including the potential matrix (19) is practically impossible due to insuperable mathematical and numerical problems. Therefore, it is desirable to develop approximative versions of these formulas. Such an approximation was presented in 1985 by Sormann and Puff⁴³ and is called the *quasifree* Bloch-modified ladder expansion. Mathematically, the QF BML expansion can be easily obtained from Eqs. (15) and (16) by using the two following approximations.

(i) All eigenenergies of the *unoccupied* electron and positron wave functions are approximated by the Sommerfeld-like expressions

$$E_{i\mathbf{k}} \approx E_{10} + \alpha_e |\mathbf{k} + \mathbf{K}_i|^2, \quad E_{j\mathbf{q}}^+ \approx E_{10}^+ + \alpha_p |\mathbf{q} + \mathbf{K}_j|^2, \quad (26)$$

where E_{10} and E_{10}^+ mean the electron and positron bottom energies and the \mathbf{K}_i and \mathbf{K}_j are the reciprocal-lattice vectors that belong to the i th and j th empty electron or positron band, respectively. The corresponding wave functions

$$\psi_{i\mathbf{k}}(\mathbf{r}) \approx \frac{1}{\sqrt{\Omega}} e^{i(\mathbf{k} + \mathbf{K}_i) \cdot \mathbf{r}},$$

$$\varphi_{j\mathbf{q}}(\mathbf{r}) \approx \frac{1}{\sqrt{\Omega}} e^{i(\mathbf{q} + \mathbf{K}_j) \cdot \mathbf{r}}$$

have Fourier coefficients

$$a_{i\mathbf{k}}(\mathbf{K}) = \delta_{\mathbf{K}, \mathbf{K}_i}, \quad b_{j\mathbf{q}}(\mathbf{K}) = \delta_{\mathbf{K}, \mathbf{K}_j}. \quad (27)$$

As can be seen from Eq. (26), all lattice effects included in the unoccupied electron and positron states are roughly approximated by the parameters α_e and α_p .

(ii) The electron-positron interaction matrix is approximated by

$$V_{\mathbf{G}_1, \mathbf{G}_2}^{ep}(\mathbf{q}) \approx V^{ep}(|\mathbf{q} + \mathbf{G}_1|; N_{\text{eff}}) \delta_{\mathbf{G}_1, \mathbf{G}_2}, \quad (28)$$

i.e., all off-diagonal elements of the matrix are neglected, which means that local-field effects of the e - p interaction are not taken into account (compare the discussion about this point in Sec. V). Additionally, the diagonal elements are approximated by a scalar interaction potential as it is used in the jellium theory, with the consequence that all lattice effects on the polarization of the electron gas are only repre-

sented by the quantity N_{eff} , which is the effective number of electrons per unit cell that contribute to the polarization. This neglect of all local-field effects of the e - p interaction is the most problematic feature of the QF BML approximation and is in complete contrast to the LDA.

Inserting the approximations (26)–(28) into the BML formulas (15) and (16), one obtains the relatively simple expressions^{43,50}

$$\begin{aligned} \rho_{2\gamma}^{\text{QF BML}}(\mathbf{k}+\mathbf{G}) &= \sum_n \Theta(E_F - E_{n\mathbf{k}}) \left\{ \sum_{\mathbf{K}} a_{n\mathbf{k}}(\mathbf{K}) b_{10}(\mathbf{G}-\mathbf{K}) \right. \\ &\quad \times \left[1 + \frac{1}{\Omega} \sum_{\mathbf{k}'} \Theta(k' - k_0) V^{ep}(|\mathbf{k}-\mathbf{k}' \right. \\ &\quad \left. \left. + \mathbf{K}; N_{\text{eff}}) \chi_{\mathbf{k};\mathbf{G}}^{\text{QF BML}}(\mathbf{k}') \right]^2 \right\}, \end{aligned} \quad (29)$$

with

$$k_0 = [(E_F - E_{10})/\alpha_e]^{1/2}, \quad (30)$$

and the corresponding Bethe-Goldstone equation

$$\begin{aligned} \chi_{\mathbf{k};\mathbf{G}}^{\text{QF BML}}(\mathbf{k}') &= (E_{n\mathbf{k}} - E_{10} - \alpha_e k'^2 - \alpha_p |\mathbf{k} + \mathbf{G} - \mathbf{k}'|^2)^{-1} \\ &\quad \times \left\{ 1 + \frac{1}{\Omega} \sum_{\mathbf{k}''} \Theta(k'' - k_0) V^{ep}(|\mathbf{k}' - \mathbf{k}''|; N_{\text{eff}}) \right. \\ &\quad \left. \times \chi_{\mathbf{k};\mathbf{G}}^{\text{QF BML}}(\mathbf{k}'') \right\}. \end{aligned} \quad (31)$$

The QF BML approach represented a successful attempt to obtain a practically feasible version of the BML theory that could be used for theoretical enhancement calculations.^{43,50,52,53}

For a further development of the BML approach, which is the main topic of this paper, the QF BML approximation gained further importance by a more sophisticated treatment of the parameters α_e , α_p and N_{eff} , which occur in Eqs. (29)–(31). This treatment of the problem leads to another version of the BML approach, which we call the *optimized* Bloch-modified ladder theory.

VII. THE OPTIMIZED BML APPROXIMATION

A. Optimization of the parameters N_{eff} , α_e , and α_p

The major problem in order to go beyond the QF BML theory is the following. How can we determine the parameters α_e , α_p , and N_{eff} that occur in Eqs. (29)–(31) such that, despite the approximations described in the preceding section, the lattice effects are taken into account as realistically as possible?

We start with the first term of the Bethe-Goldstone amplitude of the BML theory, which gives, according to Eq. (16),

$$\chi_{i,j;\mathbf{G}}^{\text{BML}}(\mathbf{k}') = \sum_{\mathbf{K}_1} a_{i\mathbf{k}'}(\mathbf{K}_1) b_{j\mathbf{q}}(\mathbf{G}-\mathbf{K}_1+\mathbf{L}) + \dots,$$

with $\mathbf{q} = \mathbf{k} - \mathbf{k}' - \mathbf{L}$ an element of the first BZ. Inserting this expression into Eq. (15), one gets

$$\begin{aligned} \rho_{2\gamma}^{\text{BML}}(\mathbf{k}+\mathbf{G}) &= \sum_n \Theta(E_F - E_{n\mathbf{k}}) [\sigma(n\mathbf{k}; \mathbf{G}) \\ &\quad + \lim_{M \rightarrow \infty} \tau_M(n\mathbf{k}; \mathbf{G})]^2 + \dots, \end{aligned} \quad (32)$$

with

$$\sigma(n\mathbf{k}; \mathbf{G}) = \sum_{\mathbf{K}} a_{n\mathbf{k}}(\mathbf{K}) b_{10}(\mathbf{G}-\mathbf{K}) \quad (33)$$

and

$$\begin{aligned} \tau_M(n\mathbf{k}; \mathbf{G}) &= \frac{1}{\Omega} \sum_{i=1}^M \sum_{\mathbf{k}'} \Theta(E_{i\mathbf{k}'} - E_F) \\ &\quad \times \sum_{j=1}^{\infty} \left[\sum_{\mathbf{K}_1} a_{i\mathbf{k}'}(\mathbf{K}_1) b_{j\mathbf{q}}(\mathbf{G}-\mathbf{K}_1+\mathbf{L}) \right] \\ &\quad \times (E_{n\mathbf{k}} - E_{i\mathbf{k}'} + E_{10}^+ - E_{j\mathbf{q}}^+)^{-1} \\ &\quad \times \sum_{\mathbf{G}_1} \sum_{\mathbf{G}_2} V_{\mathbf{G}_1, \mathbf{G}_2}^{ep}(\mathbf{q}) \left[\sum_{\mathbf{K}_2} a_{n\mathbf{k}}(\mathbf{K}_2) a_{i\mathbf{k}'}(\mathbf{K}_2 \right. \\ &\quad \left. - \mathbf{G}_1 + \mathbf{L}) \right] \left[\sum_{\mathbf{K}_3} b_{10}(\mathbf{K}_3) b_{j\mathbf{q}}(\mathbf{K}_3 + \mathbf{G}_2) \right]. \end{aligned} \quad (34)$$

In Eq. (32), σ represents the independent-particle part and τ_M is the first-order term with respect to the e - p interaction potential with M the number of unoccupied electron bands taken into consideration. These two expressions can be numerically evaluated with some expense, but without any additional approximation. Some numerical aspects and problems of this evaluation are summarized in Sec. VII C of this paper.

Now we are going to reduce Eq. (34) to the corresponding QF expression. We do this in two steps. First, we apply the approximation (28) for the e - p interaction potential, which immediately leads to the result

$$\begin{aligned} \hat{\tau}_M(n\mathbf{k}; \mathbf{G}) &= \frac{1}{\Omega} \sum_{i=1}^M \sum_{\mathbf{k}'} \Theta(E_{i\mathbf{k}'} - E_F) \\ &\quad \times \sum_{j=1}^{\infty} \left[\sum_{\mathbf{K}_1} a_{i\mathbf{k}'}(\mathbf{K}_1) b_{j\mathbf{q}}(\mathbf{G}-\mathbf{K}_1+\mathbf{L}) \right] \\ &\quad \times (E_{n\mathbf{k}} - E_{i\mathbf{k}'} + E_{10}^+ - E_{j\mathbf{q}}^+)^{-1} \\ &\quad \times \sum_{\mathbf{G}_1} V^{ep}(|\mathbf{q} + \mathbf{G}_1|; N_{\text{eff}}) \\ &\quad \times \left[\sum_{\mathbf{K}_2} a_{n\mathbf{k}}(\mathbf{K}_2) a_{i\mathbf{k}'}(\mathbf{K}_2 - \mathbf{G}_1 + \mathbf{L}) \right] \\ &\quad \times \left[\sum_{\mathbf{K}_3} b_{10}(\mathbf{K}_3) b_{j\mathbf{q}}(\mathbf{K}_3 + \mathbf{G}_1) \right]. \end{aligned} \quad (35)$$

As a second step, we also use the approximations (26) and (27), where all electron and positron scattering states are

replaced by quasifree states and we obtain, after some non-trivial but elementary manipulations, the QF approximation of τ_M ,

$$\begin{aligned} \tau_M^{\text{QF}}(n\mathbf{k};\mathbf{G}) &= \frac{1}{(2\pi)^3} \sum_{\mathbf{K}} a_{n\mathbf{k}}(\mathbf{K}) b_{10}(\mathbf{G}-\mathbf{K}) \\ &\times \int d^3k' \frac{V^{ep}(|\mathbf{k}-\mathbf{k}'+\mathbf{K}|; N_{\text{eff}})}{E_{n\mathbf{k}}-E_{10}-\alpha_e k'^2-\alpha_p |\mathbf{k}+\mathbf{G}-\mathbf{k}'|^2}, \end{aligned} \quad (36)$$

with the condition $k_0 \leq |\mathbf{k}'| \leq k_{\text{max}}(M)$ and with k_0 given by Eq. (30). The integral over \mathbf{k}' requires a comment: it has to be calculated over M Brillouin zones: the central one, and $M-1$ zones around. In our calculation, we reset this relatively complicated region by a sphere of the same volume with the radius

$$k_{\text{max}}(M) = \left(M \frac{3}{4\pi} \Omega_{\text{BZ}} \right)^{1/3},$$

where Ω_{BZ} is the (reciprocal) volume of the first BZ.

An important question concerning the numerical evaluation of Eqs. (34) and (35) is the convergence of these functions with respect to the sums Σ_i and Σ_j over the unoccupied electron and positron bands, respectively. As we shall demonstrate in Sec. VII C, the convergence with respect to the unoccupied positron bands is satisfactory. However, this is by no means the case for the unoccupied electron bands. In fact, for each theoretical approach that claims to describe the electron-scattering states realistically, the poor convergence of the sum Σ_i in Eqs. (34) and (35) is a crucial obstacle to overcome. Of course, it is reasonable to expect that the higher the electron bands lie above the Fermi level, the better these bands can be approximated by free-particle bands. Therefore, the simplest procedure would be as follows: one calculates the sum over the unoccupied electron bands up to a certain band number M using realistic Bloch states and continues the calculation analytically by approximating the higher electron and positron bands by plane waves. Such a procedure was used in the paper of Boroński and Jarlborg.⁵⁴

For the present contribution, we use a somewhat different and more reliable procedure: we numerically evaluate both the complicated formula for $\tau_M(n\mathbf{k};\mathbf{G})$ [Eq. (34)] and the corresponding parametrized approximations $\hat{\tau}_M(n\mathbf{k};\mathbf{G})$ [Eq. (35)] and $\tau_M^{\text{QF}}(n\mathbf{k};\mathbf{G})$ [Eq. (36)] as functions of the number M of unoccupied electron bands taken into account. Then, for an optimization of the parameters N_{eff} , α_e , and α_p , we perform the following two-step process: (i) we optimize the parameter N_{eff} by a least-squares (LS) comparison of the τ_M and $\hat{\tau}_M$ curves (henceforth, this optimized parameter is called $N_{\text{eff}}^{\text{BML}}$) and (ii) we optimize the parameters α_e and α_p by a LS comparison of the τ_M and τ_M^{QF} curves using $N_{\text{eff}}^{\text{BML}}$.

This two-step procedure has to be done for each initial (occupied) electron state $|n\mathbf{k}\rangle$ and for each reciprocal-lattice vector \mathbf{G} under investigation. As a result, we get the momentum- and band-dependent parameters $N_{\text{eff}}^{\text{BML}}(n\mathbf{k};\mathbf{G})$, $\alpha_e(n\mathbf{k};\mathbf{G})$, and $\alpha_p(n\mathbf{k};\mathbf{G})$. Here it has to be emphasized that, according to the procedure described above, the α_e and

α_p are influenced by several lattice effects, namely, by lattice effects (i) on the electron and positron energy levels, (ii) on the electron and positron Bloch waves, and also (iii) on the shape of the Fermi surface of the crystal electrons. This last influence can directly be seen by the fact that the effective Fermi momentum k_0 [Eq. (30)] used in the QF BML expression is a function of α_e and is therefore also momentum and band dependent. For these reasons, the parameters α_e and α_p must not be simply interpreted as inversely proportional to electron and positron band masses as it might be expected at first sight from the analytical form of Eq. (26). The momentum dependence of the optimized parameters $N_{\text{eff}}^{\text{BML}}$, α_e , and α_p for Al, Cu, Pd, Mn, and V is discussed in more detail at the end of Secs. VIII D 1 and VIII D 2 of this paper.

Now we reset the very complicated exact BML expressions (15) and (16) by the corresponding QF BML expressions (29)–(31) including the optimized parameters $N_{\text{eff}}^{\text{BML}}$, α_e , and α_p with respect to all orders of the Bethe-Goldstone amplitude. This procedure, which we call the *optimized* BML theory, contains both types of lattice effects discussed in Sec. II more realistically than any other actual theoretical approach dedicated to this problem. If we say “more realistically” we want to express that the OBML procedure is more efficient for a theoretical description of lattice effects influencing the e - p annihilation in metals than the LDA or previous formulations of the BML approach. This pretension shall be justified in the following.

As described above, the LS process, which leads to the band- and momentum-dependent parameters $N_{\text{eff}}^{\text{BML}}$, α_e , and α_p , is based on the Born approximation, i.e., on the BML and QF BML quantities τ_M , $\hat{\tau}_M$, and τ_M^{QF} [according to Eqs. (34), (35), and (36), respectively], which are all of first order with respect to the e - p interaction potential. It is therefore no surprise that the use of these parameters in the OBML theory gives excellent agreement with the corresponding exact BML theory, as long as we use the Born approximation. As we have proved by a great number of numerical tests, this is valid for all metals and for all momenta investigated, both within the central-momentum region and within the near-unklapp regions. An example of these tests will be presented in Sec. VII B.

Of course, one must be aware that the parameters described above might be less effective for higher-order ladder terms of the exact BML expansion than for the first-order term. Nevertheless, if we compare this term with the terms of order greater than 2 with respect to V^{ep} according to Eqs. (15) and (16), we see that, apart from some additional features that appear in the higher-order terms (in particular, sums of products of Fourier coefficients of unoccupied electron wave functions and also of unoccupied positron wave functions), the mathematical structure of these terms is rather similar to the ladder term of first order. Due to this similarity, one can assume that the use of $N_{\text{eff}}^{\text{BML}}$, α_e , and α_p in all terms of the ladder expansion will not seriously deteriorate the reliability of the MDAP and enhancement results obtained by the OBML theory, especially if the terms of order greater than 1 with respect to V^{ep} play only a subordinate role in the MDAP calculation.

Due to enormous numerical problems, it is not possible to check the amount of the contribution of higher-order terms

for the exact BML theory; therefore, we studied this question for the mathematically simpler LDA. For this purpose, we evaluated the LDA formula in the Born approximation, i.e., we included in Eq. (10) the local enhancement factor

$$g(\mathbf{r}; n\mathbf{k}) = \epsilon_{\text{hom}}^{\text{Born}}[r_s(\mathbf{r}); X_{n\mathbf{k}}] \quad (37)$$

and we compared these results with the corresponding MDAP values obtained by the ‘‘complete’’ LDA according to Eqs. (10) and (11). What we learned from this test is that, at least concerning the LDA, for all metals and annihilation momenta investigated in this paper, the contribution of the sum of all ladder terms of order greater than 1 with respect to V^{ep} to the MDAP is only about 30%, which means that the contribution of the first-order term (according to the Born approximation) amounts to about 70% and is therefore by far the dominant one. This marked dominance of the first-order ladder term is typical for metals in the high and medium electron density regime, i.e., with small values of the density parameter r_s , as is the case for all metals investigated in this paper. It is very important to emphasize here that this argument is valid not only for the average electron densities of these metals, but also from the point of view of their *local* electron densities. For example, even in the outer parts of the Wigner-Seitz cell of copper where the density of the d electrons is very small, the local value of r_s that is due to the single $4s$ electron does not exceed 2.7 a.u. Due to the fact that, apart from all interesting differences between the LDA and BML enhancement factors, which are the main topic of this paper, the LDA and BML results are at least principally comparable, it is justified to assume that this dominance of the first-order ladder term will be also a general feature of the BML theory. As a consequence of these results, we think that it is acceptable to use the optimized parameters $N_{\text{eff}}^{\text{BML}}$, α_e , and α_p for terms of all orders of the OBML approach, especially for metals with high and medium valence electron densities. However, it is important to mention that the dominance of the ladder term of first order with respect to V^{ep} is dramatically reduced for metals with lower average or local electron densities (higher r_s values). For example, for sodium with $r_s = 3.9$ a.u., the contribution of the first-order term to the MDAP amounts only about 30% and the situation is even worse for metals such as potassium ($r_s = 4.9$ a.u.) or rubidium ($r_s = 5.2$ a.u.). According to the argumentation of this subsection, the application of our OBML method on such metals may possibly lead to erroneous answers and is therefore not recommended.

B. Applicability of the optimization process

The central idea of the method described in the preceding subsection is an extrapolation of τ_M [Eq. (34)] ($M = 1$ up to a finite value of about 50–60) by the mathematically simpler expression τ_M^{QF} [Eq. (36)] for $M \rightarrow \infty$, including the optimized parameters $N_{\text{eff}}^{\text{BML}}$, α_e , and α_p . It is therefore of fundamental importance for the reliability of our OBML theory that this extrapolation of τ_M by τ_M^{QF} is as perfect as possible concerning both the values and the slopes of these functions. For this reason, we checked the applicability of the optimi-

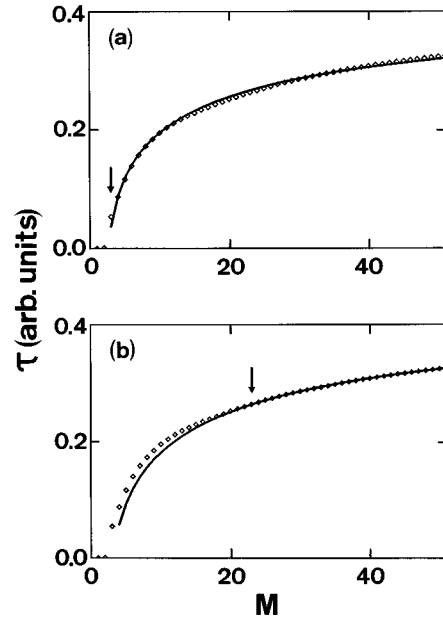


FIG. 1. Correspondence of τ_M^{QF} (solid lines) and τ_M (\diamond) according to Eqs. (36) and (34), respectively. M is the number of unoccupied electron bands included into the calculation and the arrows indicate that the LS process was started (a) at $M=3$ and (b) at $M=23$.

zation process for the OBML parameters carefully by a large number of numerical tests. What we found out is that the agreement between the τ_M^{QF} and τ_M curves is generally excellent for higher unoccupied electron bands, i.e., for $M \gg 1$. As we shall show for a typical example in Figs. 1 and 2, according to some details of this optimization process described below, significant deviations between τ_M^{QF} and τ_M may appear for small values of M , i.e., for electron scattering bands lying closely above the Fermi energy. We emphasize here that this does not mean that our optimized BML parameters are insufficient in describing the contributions of these scattering bands to τ_M . Namely, it is not important that the two curves τ_M and τ_M^{QF} agree for the contribution of *any* scattering band. Decisive is only that both curves represent, as well as possible, the same sum over all contributions of all scattering bands and, consequently, lead to the same values of the MDAP and the enhancement factor.

As a typical example, this behavior is demonstrated for Pd for the initial electron state $|10\rangle$, i.e., for the lowest valence band at the Γ point of the BZ. As we mentioned above, a free-electron-like behavior of the electron scattering bands can only be expected far above E_F for relatively high band numbers. The consequence of this fact is that one should avoid starting the LS comparison between τ_M and τ_M^{QF} at too small values of M . This is demonstrated in Figs. 1 and 2, where we present τ_M and τ_M^{QF} as functions of M . For Fig. 1(a), the LS process was started at $M = 3$ (indicated by an arrow) and yielded good overall agreement between the τ_M and τ_M^{QF} curves. Nevertheless, one observes that the slope of the τ_M^{QF} curve for the region of higher M becomes significantly smaller than the slope of the corresponding τ_M curve. In our test calculations for the $|10\rangle$ electron state in Pd, we

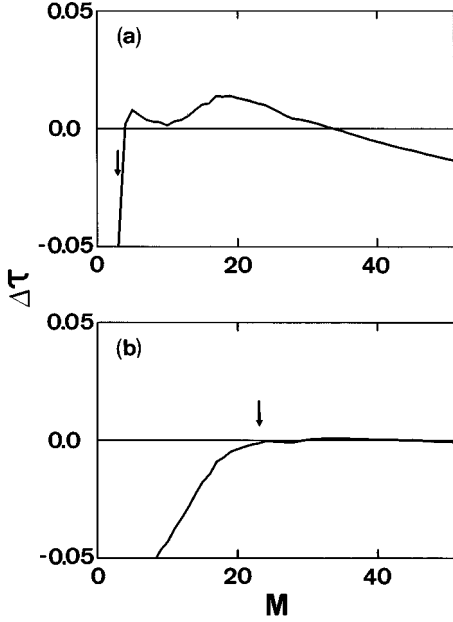


FIG. 2. $\tau_M^{\text{QF}} - \tau_M$ in units of τ_M for the maximum value of M , with τ_M^{QF} and τ_M according to Eqs. (36) and (34), respectively. M is the number of unoccupied electron bands included into the calculation and the arrows indicate that the LS process was started (a) at $M=3$ and (b) at $M=23$.

estimated an error of about 8% for the enhancement factor due to this imperfect extrapolation. This behavior is even better observable in Fig. 2(a), where we show the relative difference between τ_M^{QF} and τ_M as a function of M . If, however, the LS process is started at a higher value of M [$M = 23$ in our example, see Figs. 1(b) and 2(b)], deviations between τ_M^{QF} and τ_M for the scattering bands immediately above E_F appear due to lattice effects, but, on the other hand, we achieve an almost ideal agreement of the two curves for $M \gg 1$ for both their values and their slopes, which guarantees a reliable extrapolation process.

As a summary of our tests we can say that the optimization process for $N_{\text{eff}}^{\text{BML}}$, α_e , and α_p presented in Sec. VII A leads to satisfying (and in most cases excellent) agreement between the BML theory and the (mathematically much simpler) QF BML approach for all metals investigated and not only for initial electron states inside the first BZ but also for states in the umklapp regions.

C. Numerical evaluation of $\tau_M(n\mathbf{k};\mathbf{G})$

Before we present a discussion about our enhancement results, we think it is useful to refer at least some important aspects of the numerical evaluation of the relatively complicated expression $\tau_M(n\mathbf{k};\mathbf{G})$ given in Eq. (34). All plane-wave coefficients of the (occupied and unoccupied) electron and positron states used in our calculations were obtained by Fourier expansions [see Eqs. (13) and (14)] of the corresponding wave functions, which were calculated by a conventional augmented-plane-wave program. For each Bloch vector, single-particle eigenenergies for up to 80 electron and positron bands were determined by a self-consistent solution of the Schrödinger-like equations (6) and (7). Concerning the

exchange-correlation parts of the crystal potentials, in the electron case, we used the parametrized approximation by Hedin and Lundqvist.⁷⁰ In the case of the positron, all self-energy correlation parts of the crystal potential were neglected (see our discussion about this point in Sec. II). No relativistic corrections to the crystal potentials, in particular no spin-orbit corrections, were taken into account.

In order to check the numerical reliability of our results, we performed extensive convergence tests for the quantities $\sigma(n\mathbf{k};\mathbf{G})$ and $\tau_M(n\mathbf{k};\mathbf{G})$ defined in Eqs. (33) and (34), respectively. It was the aim of these test calculations to guarantee that the numerical accuracy of our BML results was, for all values of the MDAP except values that are very low in magnitude, better than 3%. This does not sound very ambitious, but due to the high numerical expense of the BML method it is not realistic to aspire to a higher accuracy. It is impossible to report all these tests in detail, but we shall give here at least an overview.

Equations (33)–(36) contain sums of products of electron-positron, electron-electron, and positron-positron Fourier coefficients. The question was how many terms have to be included into the evaluation of these sums. It was also important to know how many reciprocal-lattice vectors \mathbf{G}_1 and \mathbf{G}_2 had to be used for the sums in Eqs. (34) and (35). We obtained that, for the accuracy mentioned above, it was sufficient to use about 200 Fourier coefficients for each electron and positron Bloch state and about 130 vectors $\mathbf{G}_1, \mathbf{G}_2$.

Another important influence on the quality of the numerical evaluation of Eqs. (34) and (35) is given by the number of Bloch vectors \mathbf{k}' used for the sum over the unoccupied part of the first BZ. This summation, which was done by the use of the well-known integration method of Gilat and Raubenheimer,⁷¹ required only a relatively small number of primary \mathbf{k}' points within the irreducible wedge (IW) of the BZ, namely, 40 (70) \mathbf{k}' vectors for the electron states and 112 (125) \mathbf{k}' vectors for the positron states in bcc (fcc) structures. A special difficulty is caused by the fact that, for an average value of the momentum vector \mathbf{k} , the resulting Bloch vector $\mathbf{q} = \mathbf{k} - \mathbf{k}' - \mathbf{L}$ for the positron states in Eqs. (34) and (35) does not necessarily coincide with one of the precalculated primary \mathbf{k}' points within the IW. We solved this problem by a combination of Gilat and Raubenheimer's scheme and the well-approved $\mathbf{k} \cdot \mathbf{p}$ interpolation method.⁷² To save computer time, all symmetry properties of the crystal lattice were carefully taken into account.

The accuracy of the components of the matrix $V_{\mathbf{G}_1, \mathbf{G}_2}^{ep}$ of the electron-positron interaction potential plays an important role for the good quality of the numerical results of $\tau_M(n\mathbf{k};\mathbf{G})$. In agreement with Hybertsen and Louie,⁶⁸ we also realized that the most crucial point of the numerical calculation of these matrix elements is to secure the convergence of the sum over unoccupied electron bands in the expression (24) for the polarizability matrix P . In our calculations, we used 60–70 unoccupied electron bands and achieved a convergence of most of the matrix elements of V^{ep} within a few percent (see Table I), except for very small elements with negligible influence on the MDAP results. For such components, relative errors of 100% and more may appear.

TABLE I. Selected elements of the electron-positron interaction matrix $-V_{\mathbf{G}_1, \mathbf{G}_2}^{ep}(\mathbf{k})$ for vanadium as functions of the number of unoccupied electron bands taken into account for the numerical evaluation of Eq. (24). The Bloch vector \mathbf{k} lies at the N point on the boundary of the Brillouin zone.

\mathbf{G}_1	\mathbf{G}_2	34 bands	49 bands	63 bands
000	000	0.4360	0.4350	0.4348
110	110	0.1918	0.1896	0.1890
220	220	0.0784	0.0782	0.0781
110	$\bar{1}\bar{1}0$	-0.0096	-0.0092	-0.0090
200	$\bar{1}\bar{1}0$	-0.0082	-0.0083	-0.0084
220	$\bar{1}\bar{1}2$	0.00032	0.00027	0.00026
110	$\bar{1}\bar{1}\bar{2}$	-0.00012	-0.000080	-0.000019

In Sec. VII A we already discussed the insufficient convergence of τ_M with respect to the number M of unoccupied electron bands taken into account and we also proposed a way to overcome this difficulty. Fortunately, this problem does not arise for the sum over unoccupied positron bands: as a result of our tests, we obtained that the convergence with respect to these bands is well established in all cases investigated in this paper. Some test results that demonstrate this positive behavior are summarized in Table II, where we show the dependence of $\tau_M(n\mathbf{k}; \mathbf{G})$ for different metals and different initial electron states $|n\mathbf{k}\rangle$ on the number J of positron bands taken into account, calculated for a fixed number M of unoccupied electron bands.

VIII. RESULTS AND DISCUSSION

A. The e - p interaction potential

All results presented in this paper are based on the *static* RPA for the effective e - p interaction potential. Such a procedure, which ignores the existence of better approximations for this potential^{3,73} requires some justification. The reason is that, for the present investigation, we were especially interested in a comparison of BML and LDA enhancement factors and we found that the relations between these two types of results do not significantly depend on the approximation

TABLE II. Demonstration of the convergence of τ_M according to Eq. (34) with fixed M and with respect to the number J of positron scattering bands. (a) Copper: $\mathbf{k}=(0.820,0,0)$, second band, $M=51$. (b) Vanadium: $\mathbf{k}=(0.247,0.247,0)$, second band, $M=70$. k is in units of $2\pi/a$ with $a=6.8308$ and 5.7145 a.u. for Cu and V, respectively.

(a)		(b)	
J	t	J	t
35	0.368	51	0.0869
40	0.373	56	0.0879
45	0.376	61	0.0886
50	0.379	66	0.0890
55	0.382	71	0.0892
60	0.383	76	0.0894
65	0.384	81	0.0895
70	0.384	86	0.0895

for V^{ep} . On the other hand, the use of a RPA potential considerably simplified our calculations. Therefore, for all results presented in the following, we used the matrix of the e - p potential according to static approximations of Eqs. (20) and (21) in Sec. V in connection with the RPA for the polarizability matrix, given by Eqs. (22)–(25). Of course, in order to compare commensurable BML and LDA results, we also had to evaluate the LDA expression (10) with the pair-correlation function in the RPA, namely,

$$g(\mathbf{r}; n\mathbf{k}) = \epsilon_{\text{hom}}^{\text{RPA}}[r_s(\mathbf{r}); X_{n\mathbf{k}}].$$

Further remarks on the e - p interaction potential in real metals, in particular concerning approximations of V^{ep} ‘‘beyond the RPA’’ and the inclusion of dynamical aspects, are given in Appendix A.

B. The choice of the test metals

In the following, we shall discuss results of our recent investigations on positron enhancement in a simple metal (aluminum), a noble metal (copper), and three transition metals (palladium, bcc manganese, and vanadium). The choice of these metals is by no means arbitrary but is motivated by their different electron band structures and corresponding density of states (DOS).⁷⁴

The DOS curve for Al with its three valence electrons is, of course, very similar to the free-electron case. The two valence bands (the lower one is completely occupied and the higher one is partially occupied) have predominantly sp character with a relatively small addition of a d character. The electronic structure of all other metals investigated is more or less strongly influenced by d bands and it is one of the main purposes of our work to investigate how the lattice effects acting on the enhancement factors in these metals depend on the energetic position of the d bands with respect to E_F . For Cu, the upper edge of the d bands lies about 0.15 Ry below E_F . In the case of Pd, the Fermi level is localized just below the upper edge of the d bands, whereas in bcc Mn, a considerable part of the d -band DOS lies above E_F , a situation that is even more pronounced in V, where the greatest part of the d bands is unoccupied. Therefore, we would expect that deviations of the rate enhancement from the free-electron (jellium) case increase along the series Al \rightarrow Cu \rightarrow Pd \rightarrow Mn \rightarrow V, and this is, in principle, exactly what we learn from our results.

Concerning the occupied (initial) electron states $|n\mathbf{k}\rangle$, we performed our calculations for the fcc metals Al, Cu, and Pd along the [111] direction and for the bcc metals Mn and V along the [110] direction in momentum space. Additionally, for all occupied electron states investigated, we analyzed the character of each state with respect to the quantum number l of the orbital angular momentum.

Additionally, it results that for the metals and momentum directions investigated, there are only two totally or partially occupied valence electron bands that contribute to the MDAP. In Figs. 3 and 4, where we show the electron band structures for Al, Cu, and Pd along the ΓL direction and for Mn and V along the ΓN direction, these bands are indicated by the numbers 1 and 2 and will be called the ‘‘first band’’ and the ‘‘second band,’’ respectively, in the following text.

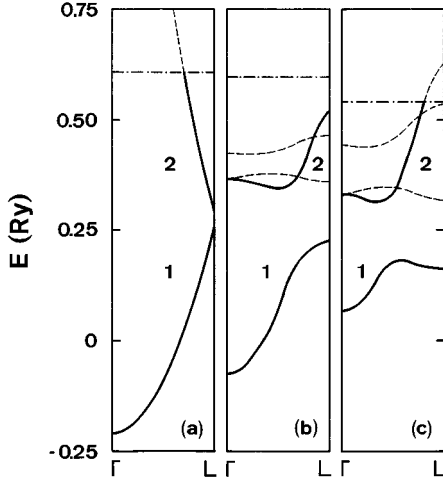


FIG. 3. Electron band structures of (a) Al, (b) Cu, and (c) Pd along the [111] direction in momentum space. The occupied parts of the bands whose electrons contribute to the MDAP are indicated by thick solid lines and by the numbers 1 and 2. The horizontal dash-dotted lines denote the Fermi energies.

C. Three types of enhancement factors

The results of our investigation are presented in the Figs. 5–17, where we show theoretical state-dependent enhancement factors for annihilation vectors $\mathbf{k} + \mathbf{G}$ with \mathbf{k} an element of the first BZ and both $\mathbf{G} = \mathbf{0}$ (LMC) and $\mathbf{G} \neq \mathbf{0}$ (HMC). The partial enhancement factors belonging to the n th band are defined by

$$\epsilon(n; \mathbf{k} + \mathbf{G}) = \rho_{2\gamma}(n; \mathbf{k} + \mathbf{G}) / \rho_{2\gamma}^{\text{IPM}}(n; \mathbf{k} + \mathbf{G}),$$

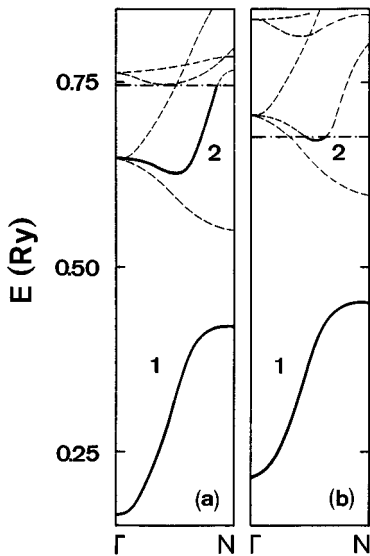


FIG. 4. Electron band structures of (a) Mn and (b) V along the [110] direction in momentum space. The occupied parts of the bands whose electrons contribute to the MDAP are indicated by thick solid lines and by the numbers 1 and 2. The horizontal dash-dotted lines denote the Fermi energies.

with $\rho_{2\gamma}(n; \mathbf{k} + \mathbf{G})$ and $\rho_{2\gamma}^{\text{IPM}}(n; \mathbf{k} + \mathbf{G})$ the contributions of the n th occupied electron band to the MDAP including and excluding the electron-positron interaction, respectively, and $\rho_{2\gamma}^{\text{IPM}}$ given by Eq. (9).

As we extensively discussed in Sec. II, the BML enhancement contains two different types of lattice effects, which we called the lattice effect on the e - p scattering and the lattice effect on the polarization. For a proper physical interpretation of our results, it is desirable to distinguish between these two types of effects. For this purpose, we define the following three enhancement factors.

(i) The LDA enhancement factor

$$\epsilon^{\text{LDA}}(n; \mathbf{k} + \mathbf{G}) = \rho_{2\gamma}^{\text{LDA}}(n; \mathbf{k} + \mathbf{G}) / \rho_{2\gamma}^{\text{IPM}}(n; \mathbf{k} + \mathbf{G}), \quad (38)$$

with $\rho_{2\gamma}^{\text{LDA}}$ as given in Eqs. (10)–(12). This enhancement factor contains none of the lattice effects defined in Sec. II.

(ii) The second enhancement factor used in our investigation is obtained as follows: we start from the LDA formula for the MDAP and define a state- and band-dependent effective electron density parameter $r_{s,\text{eff}}$ by the condition

$$\begin{aligned} \rho_{2\gamma}^{\text{LDA}}(n; \mathbf{k} + \mathbf{G}) &= \Theta(E_F - E_{n\mathbf{k}}) \\ &\times \left| \frac{\Omega}{\Omega_0} \int_{\Omega_0} d^3r \exp[-i(\mathbf{k} + \mathbf{G}) \cdot \mathbf{r}] \right. \\ &\times \left. \sqrt{\epsilon_{\text{hom}}[r_s(\mathbf{r}); X_{n\mathbf{k}}]} \psi_{n\mathbf{k}}(\mathbf{r}) \varphi(\mathbf{r}) \right|^2 \\ &\stackrel{!}{=} \epsilon_{\text{hom}}[r_{s,\text{eff}}(n; \mathbf{k} + \mathbf{G}); X_{n\mathbf{k}}] \\ &\times \rho_{2\gamma}^{\text{IPM}}(n; \mathbf{k} + \mathbf{G}). \end{aligned} \quad (39)$$

The corresponding effective number of electrons per unit cell Ω_0 is given by

$$N_{\text{eff}}^{\text{LDA}}(n; \mathbf{k} + \mathbf{G}) = \frac{3\Omega_0}{4\pi} \frac{1}{r_{s,\text{eff}}^3(n; \mathbf{k} + \mathbf{G})}. \quad (40)$$

Using these $N_{\text{eff}}^{\text{LDA}}$ values, one can execute the second step of the optimization process described in Sec. VII A for getting the corresponding values for the remaining parameters α_e and α_p . Surprisingly, we obtain that the differences between the α_e and α_p values belonging to the parameters $N_{\text{eff}}^{\text{BML}}$ (obtained by the LS process described in Sec. VII A) and $N_{\text{eff}}^{\text{LDA}}$ [obtained by the use of Eqs. (39) and (40)] are rather small. Therefore, in the following, we do not distinguish between the parameters $\alpha_e^{\text{BML}}, \alpha_p^{\text{BML}}$ and $\alpha_e^{\text{LDA}}, \alpha_p^{\text{LDA}}$. The enhancement factors that result from QF BML calculations including $N_{\text{eff}}^{\text{LDA}}, \alpha_e$, and α_p are called $\epsilon^{\text{scatter}}(n; \mathbf{k} + \mathbf{G})$; they can be considered as results where only the lattice effect on the e - p scattering is taken into account.

(iii) The OBML enhancement factor according to the QF BML theory including the parameters $N_{\text{eff}}^{\text{BML}}, \alpha_e$, and α_p optimized in the way described in Sec. VII A is given by

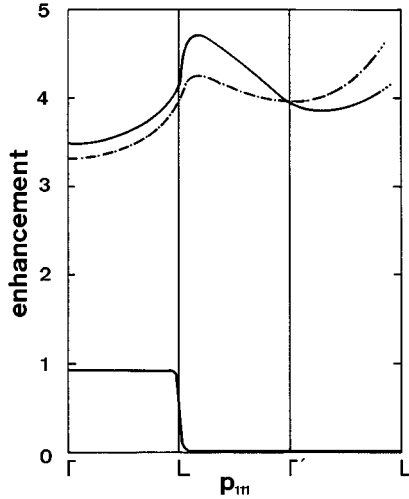


FIG. 5. State-dependent enhancement ϵ for the first band in fcc aluminum as a function of the extended momentum \mathbf{p} along the [111] direction. Solid line, enhancement $\epsilon^{\text{OBML}} \approx \epsilon^{\text{scatter}}$. Note that in this figure, these two types of enhancement curves are graphically indistinguishable. Dash-dotted line, enhancement ϵ^{LDA} . The exact meaning of ϵ^{OBML} , $\epsilon^{\text{scatter}}$, and ϵ^{LDA} is given in Sec. VIII C of this paper. Dots at the beginning or the end of enhancement curves indicate MDAP values too small for a reliable numerical determination of ϵ . The solid curve at the bottom of the figure means the MDAP according to the IPM.

$$\epsilon^{\text{OBML}}(n; \mathbf{k} + \mathbf{G}) = \rho_{2\gamma}^{\text{OBML}}(n; \mathbf{k} + \mathbf{G}) / \rho_{2\gamma}^{\text{IPM}}(n; \mathbf{k} + \mathbf{G}). \quad (41)$$

This enhancement factor contains both types of lattice effects, namely, on the e - p scattering and on the polarization of the electron gas.

The three quantities ϵ^{LDA} , $\epsilon^{\text{scatter}}$, and ϵ^{OBML} are very helpful for a relevant physical interpretation of our results, for we can say that (i) differences between $\epsilon^{\text{scatter}}$ and ϵ^{LDA} describe how the enhancement is influenced by lattice effects on the e - p scattering, (ii) differences between ϵ^{OBML} and $\epsilon^{\text{scatter}}$ give information about lattice effects on the polarization, and (iii) differences between ϵ^{OBML} and ϵ^{LDA} describe the combined effect of both types of lattice effects.

D. Discussion of the enhancement results

1. Central momentum-region

A selection of our enhancement results for the central momentum region is given in Figs. 5–10. Each figure contains the three different enhancement factors ϵ^{OBML} , $\epsilon^{\text{scatter}}$, and ϵ^{LDA} as solid, dashed, and dash-dotted lines, respectively. Additionally, at the bottom of each figure, we present the MDAP according to the IPM, where the dashed parts represent the unoccupied regions of the corresponding electron band.

Let us start with a discussion of the enhancement of the first band in Al along the [111] direction (Fig. 5). Due to its simple electron band structure (typical sp -like bands with a small content of d character of less than 10%), it is not surprising that the enhancement curves of this metal for the

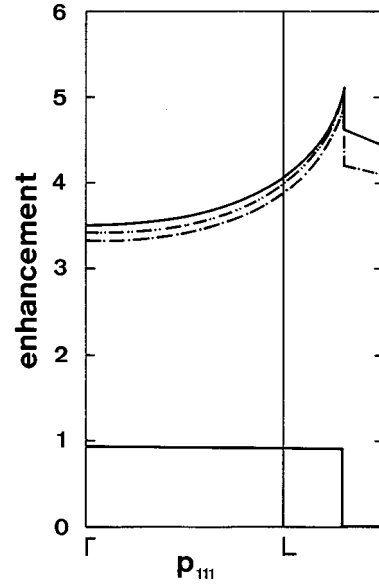


FIG. 6. Enhancement ϵ of the sum of the contributions of the first and the second band in fcc aluminum as a function of the extended momentum \mathbf{p} along the [111] direction. Solid line, enhancement ϵ^{OBML} ; dash-dotted line, enhancement ϵ^{LDA} . For comparison, the dash-double-dotted line shows the Kahana enhancement curve for the electron density parameter $r_s = 2.07$ a.u. according to a lattice constant of 7.6395 a.u. and three valence electrons per unit cell. The solid curve at the bottom of the figure means the MDAP according to the IPM.

LMC of the MDAP show the typical Kahana-like shape, i.e., a monotonic increase with increasing momentum. As explained in the preceding subsection, the influence of lattice effects on the polarization of the inhomogeneous electron gas can be studied by a comparison of the enhancements ϵ^{OBML} and $\epsilon^{\text{scatter}}$. As can be seen in Fig. 5, the corresponding curves are completely indistinguishable, which indicates that, in the case of Al, lattice effects on the polarization are almost negligible, which means that the polarization of the inhomogeneous electron gas in Al is very similar to the polarization of a homogeneous gas. This is also evident if one considers the effective number of electrons per unit cell contributing to the polarization: the $N_{\text{eff}}^{\text{LDA}}$ value extracted from LDA results (as described in Sec. VIII C) is practically independent of the momentum and amounts to 3.22, a number that agrees within 3% to the corresponding optimized BML parameter of 3.32. On the other hand, a comparison of the enhancements $\epsilon^{\text{scatter}} \approx \epsilon^{\text{OBML}}$ and ϵ^{LDA} shows that the influence of lattice effects on the e - p scattering leads to a moderate increase of the enhancement of about 5–6%.

The partly occupied second valence band of Al contains the third valence electron and therefore has its highest contribution to the MDAP outside the central BZ. This band has sp character and is, consequently, also Kahana-like enhanced. OBML and LDA enhancement results for the sum of both the first and second valence band of Al to the MDAP are presented in Fig. 6. For comparison, this figure also contains the corresponding ‘‘simple’’ Kahana enhancement curve belonging to a homogeneous electron gas with density parameter $r_s = 2.07$ a.u.

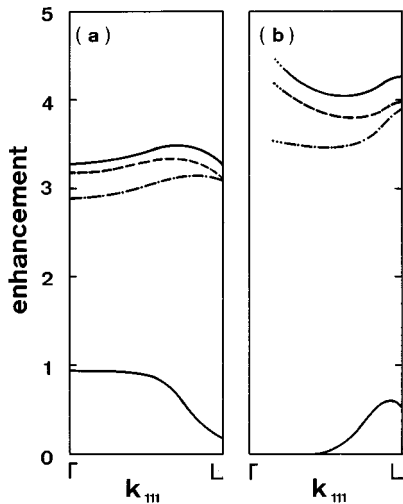


FIG. 7. State-dependent enhancement ϵ in fcc copper as a function of the reduced momentum \mathbf{k} along the [111] direction: (a) first band and (b) second band. Solid line, enhancement ϵ^{OBML} ; dashed line, BML enhancement $\epsilon^{\text{scatter}}$ including $N_{\text{eff}}^{\text{LDA}}$ according to Eqs. (39) and (40); Dash-dotted line, enhancement ϵ^{LDA} . The exact meaning of ϵ^{OBML} , $\epsilon^{\text{scatter}}$, and ϵ^{LDA} is given in Sec. VIII C of this paper. Dots at the beginning or the end of enhancement curves indicate MDAP values too small for a reliable numerical determination of ϵ . The solid curves at the bottom of the figure mean the MDAP according to the IPM.

In Figs. 7(a) and 7(b), we show enhancement factors in Cu along the [111] direction for the first and the second band, respectively. Concerning the corresponding enhancement curves, it is important to keep in mind the l character of these bands: at the Γ point in the center of the BZ, the first band starts purely s -like, but with increasing momentum the s character decreases to about 20% in favor of the d character. On the other hand, the second band starts purely d -like and becomes more and more p -like if the momentum increases (compare the band structure in Fig. 3). This behavior is clearly reflected by the corresponding enhancement curves: as long as the s or sp character of a band dominates, the enhancement is Kahana-like, as we observed for Al. However, if the d character becomes more and more dominant, the increase of ϵ with increasing momentum is strongly reduced or even converted into a decrease. Both our LDA and BML results in Cu support this interpretation (and we found this behavior, in principle, also for the other d -band metals investigated), but there are quantitative differences: the negative slope of ϵ with respect to $|\mathbf{k}|$ is significantly more marked for the BML enhancement factors than for the LDA results. A more detailed analysis of the results of Fig. 7 shows that this difference in the momentum dependence of ϵ between the LDA and BML approximation is mainly due to the lattice effect on the e - p scattering (compare the curves $\epsilon^{\text{scatter}}$ and ϵ^{LDA}), which also causes a significant increase of the enhancement for both bands investigated. The lattice effect on the polarization further increases the enhancement but does not change the momentum dependence very much. This increase of the enhancement indicates that the effective number of electrons contributing to the polarization of the electron gas in Cu is overestimated by the LDA: within the

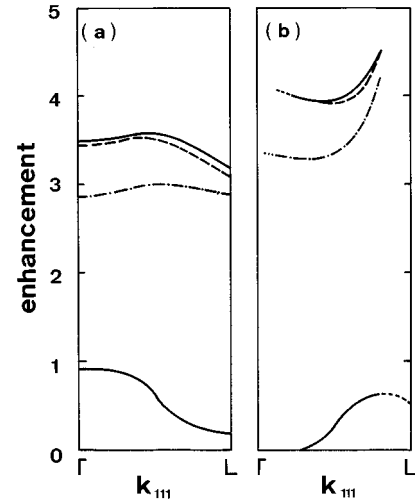


FIG. 8. State-dependent enhancement ϵ in fcc palladium as a function of the reduced momentum \mathbf{k} along the [111] direction: (a) first band and (b) second band (partially occupied). Solid line, enhancement ϵ^{OBML} ; dashed line, BML enhancement $\epsilon^{\text{scatter}}$ including $N_{\text{eff}}^{\text{LDA}}$ according to Eqs. (39) and (40); dash-dotted line, enhancement ϵ^{LDA} . The exact meaning of ϵ^{OBML} , $\epsilon^{\text{scatter}}$, and ϵ^{LDA} is given in Sec. VIII C of this paper. Dots at the beginning or the end of enhancement curves indicate MDAP values too small for a reliable numerical determination of ϵ . The curves at the bottom of the figure mean the MDAP according to the IPM, where the occupied (unoccupied) parts are given by solid (dashed) lines.

first BZ, we observed N_{eff} values between 3.1 and 3.7 for the LDA and only between 2.1 and 2.7 for our OBML approach. These smaller N_{eff} values mean a smaller effective electron density and, consequently, a higher enhancement.

The electron band structure of fcc palladium is similar to that of Cu with the important difference that the d bands lie significantly higher with respect to the Fermi energy and even slightly intersect E_F . It is interesting to investigate how these differences of the band structure affect the enhancement curves of Pd (Fig. 8). Concerning the first band in the [111] direction, the enhancement curves are, in principle, similar to the corresponding results in Cu, but with a more marked negative slope of the curves in the neighborhood of the boundary of the BZ, which probably can be attributed to a different energy dependence of the Cu and Pd bands. For the second band, however, the enhancement curves for Cu and Pd are more significantly different: as one can see by comparing Figs. 7(b) and 8(b), the enhancement in Pd is much more Kahana-like than the corresponding curve in Cu. This different behavior can also be explained by a somewhat different energy dependence of the two bands that influences their l character. For Pd, the second band comes up to the Fermi surface for $|\mathbf{k}|=0.695$ and the corresponding state has the character s - p - $d=17\%$ - 70% - 10% , i.e., it is almost purely sp -like. In the case of Cu, however, the electron state of the second band for the same value of $|\mathbf{k}|$ has the character s - p - $d=11\%$ - 59% - 27% with a percentage of d that is about three times as large as that observed for Pd. This leads to the relatively flat shape of the BML enhancement curves in Fig. 7(b). A comparison of the $\epsilon^{\text{scatter}}$ and ϵ^{LDA} curves in Fig. 8 shows a strong influence of the lattice effect on the e - p scat-

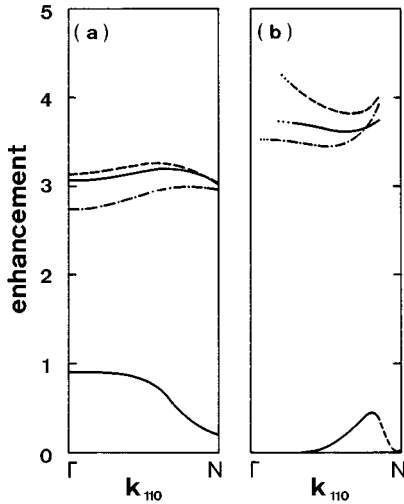


FIG. 9. State-dependent enhancement ϵ in bcc manganese as a function of the reduced momentum \mathbf{k} along the $[110]$ direction: (a) first band and (b) second band (partially occupied). The notations of this figure are the same as in Fig. 8.

tering; close to the Γ point, we observe an increase of the enhancement of about 20%. Surprising is the small difference of the ϵ^{OBML} and $\epsilon^{\text{scatter}}$ curves for the first and especially for the second band, which indicates that the effective number of polarizing electrons per unit cell is similar for the BML approximation and the LDA. So we can say that the LDA gives a good description of the polarization of the inhomogeneous electron gas in palladium. This statement is also supported by the calculated values of N_{eff} according to Eqs. (39) and (40) and the corresponding optimized BML values. For the first band of Pd, we obtained N_{eff} values between 4.3 and 4.8 for the LDA and 3.6–3.7 for the BML approximation. For the second band, the N_{eff} values are even more similar, namely, ≈ 4.1 for the LDA and ≈ 3.9 for the BML approximation.

If the different strength of the lattice effect on the polarization process in Cu and Pd has something to do with the different energetic position of the d bands with respect to E_F , this behavior can be expected to become more and more significant for manganese and vanadium, where more and more d electrons have energies higher than the Fermi energy. We shall demonstrate in the following that this expectation is fulfilled.

Figure 9 contains some results for bcc manganese, the fourth example in the series of metals investigated. For this material, a great part of the DOS of the d states is situated above the Fermi energy. Obviously, this fact does not change the momentum dependence of the enhancement drastically in comparison with the metals described before. We see that the shape of both the LDA and BML enhancement curves for Mn along the $[110]$ direction is similar to what we observed for Cu. This similarity is also evident for the influence of the lattice effect on the e - p scattering, which increases the LDA enhancement factors by about 15–20%. However, and this is important, we see that the relation between the enhancement curves including or excluding the lattice effect on the polarization is opposite the previously discussed results for Cu and Pd: here the ϵ^{OBML} curves (solid lines) lie *below* the

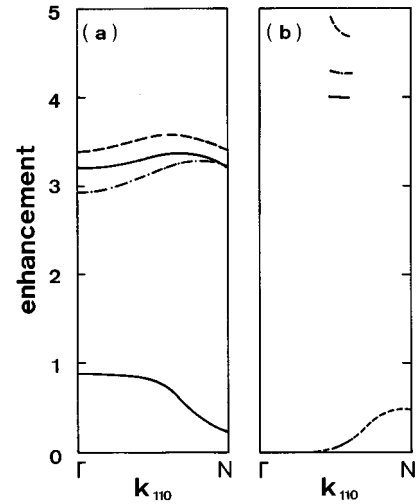


FIG. 10. State-dependent enhancement ϵ in bcc vanadium as a function of the reduced momentum \mathbf{k} along the $[110]$ direction: (a) first band and (b) second band (partially occupied). The notations of this figure are the same as in Fig. 8.

corresponding $\epsilon^{\text{scatter}}$ curves (dashed lines), i.e., in the case of Mn, the number of electrons engaged in the polarization process is underestimated by the LDA. This effect is moderate for the first band with momentum-dependent N_{eff} values between 3.9 and 4.2 and between 4.0 and 4.5 for the LDA and the BML approximation, respectively, but is rather strong for the second band with N_{eff} around 3.8 for the LDA and between 5.5 and 6.5 for the BML approximation. Unlike Cu and Pd, in manganese, the two lattice effects on the e - p scattering and on the polarization partly compensate each other, leading to a significant reduction of differences between the LDA and OBML enhancement factors.

This effect is even larger for vanadium, where the enhancement curves along $[110]$ are shown in Fig. 10. For this metal, whose d bands are mainly situated above the Fermi energy, the considerable differences between $\epsilon^{\text{scatter}}$ and ϵ^{LDA} due to lattice effects on the e - p scattering are largely compensated for the first band and even overcompensated for the second band by the influence of the lattice effect on the polarization (compare the curves for ϵ^{OBML} and $\epsilon^{\text{scatter}}$). This situation is also reflected by the N_{eff} values, which are significantly lower for the LDA than for the BML approach: for the first band along the $[110]$ direction, we obtained N_{eff} values of 3.8–4.1 for the LDA and 5.7–6.2 for the BML approximation. This effect is even more drastic for the small occupied part of the second band, which is predominantly d -like. For these initial electron states, we calculated N_{eff} values of about 3.4 for the LDA and about 8 for the BML approximation. These results indicate a marked underestimation of the effective electron density by the LDA concerning the polarization of the inhomogeneous electron gas in vanadium.

In Tables III and IV we present a summary of the band- and momentum-dependent parameters $N_{\text{eff}}^{\text{BML}}$, $N_{\text{eff}}^{\text{LDA}}$, α_e , and α_p within the central-momentum region as they were obtained by the optimization process described in Sec. VII A and Eqs. (39) and (40). The $N_{\text{eff}}^{\text{BML}}$ and $N_{\text{eff}}^{\text{LDA}}$ values of Table

TABLE III. N_{eff} values per unit cell for the polarization of the inhomogeneous electron gas in different metals within the central momentum region along the [110] and [111] directions for bcc and fcc metals, respectively. The lattice constants a are given in a.u. The $N_{\text{eff}}^{\text{BML}}$ values are results of the BML optimization described in Sec. VII A and the $N_{\text{eff}}^{\text{LDA}}$ values were extracted from LDA results according to Eqs. (39) and (40). The terms ‘‘First band’’ and ‘‘Second band’’ are explained in Sec. VIII B and in Figs. 3 and 4 of this paper. Regions of N_{eff} values in the table correspond to increasing order of momenta.

Metal	Structure	a	First band		Second band	
			BML	LDA	BML	LDA
Al	fcc	7.6395	3.32	3.22		
Cu	fcc	6.8308	2.5–2.7	3.4–3.7	2.3–2.1	3.1–3.2
Pd	fcc	7.33	3.6–3.7	4.3–4.8	3.8–4.0	4.1–4.2
Mn	bcc	5.397	4.5–4.0	3.9–4.2	6.5–5.5	3.7–3.9
V	bcc	5.7145	5.7–6.2	3.8–4.1	≈ 8.0	≈ 3.4

III have been already discussed in this subsection. Concerning the momentum dependence of the corresponding parameters α_e and α_p along the ΓL (ΓN) direction for the fcc (bcc) metals investigated, one observes almost constant values for the first band of Al and a relatively weak momentum dependence of α_e and α_p for all other metals in study, for both the first and the second band. It has already been mentioned in Sec. VIII C that the parameters α_e, α_p , which belong to the $N_{\text{eff}}^{\text{BML}}$ values, are almost (within a few percent) identical to the corresponding parameters that belong to the $N_{\text{eff}}^{\text{LDA}}$ values. Therefore, in Table IV, only the α_e and α_p values belonging to $N_{\text{eff}}^{\text{BML}}$ are shown. Due to the definition of α_e and α_p in Eq. (26), it is clear that deviations of these parameters from the unity reflect deviations of the corresponding occupied and nonoccupied electron and positron states from free-particle states. From this point of view, it is not surprising that one observes relatively small deviations of α_e, α_p from the unity for Al and Cu with their nearly free valence electron states for energies close to the Fermi energy, in some contrast to the α_e, α_p values for the transition metals Pd, Mn, and V, where the energy region around E_F is dominated by d states.

TABLE IV. α_e and α_p values according to the optimization process described in Sec. VII A for momenta within the central region along the [111] and [110] directions for fcc and bcc metals, respectively. The parameters belonging to the $N_{\text{eff}}^{\text{BML}}$ values and to the $N_{\text{eff}}^{\text{LDA}}$ values are almost identical (within a few percent). Therefore, only the α_e and α_p values that belong to the $N_{\text{eff}}^{\text{BML}}$ are presented. The terms ‘‘First band’’ and ‘‘Second band’’ are explained in Sec. VIII B and in Figs. 3 and 4 of this paper. Regions of N_{eff} values in the table correspond to increasing order of momenta.

Metal	Structure	First band		Second band	
		α_e	α_p	α_e	α_p
Al	fcc	0.86–0.89	1.02–1.03		
Cu	fcc	0.91–0.75	1.17–1.43	1.13–0.93	0.92–1.19
Pd	fcc	0.57–0.42	1.33–1.63	0.65–0.59	1.22–1.30
Mn	bcc	0.71–0.59	1.30–1.58	0.81–0.68	1.09–1.30
V	bcc	0.68–0.56	1.33–1.55	0.77–0.71	1.15–1.19

2. High-momentum region

As already mentioned in the Introduction, a second point of discussion (apart from the negative slope of momentum-dependent enhancement curves for d -like electron states) is the question whether the enhancement factors in metals are more or less the same for the LMC and the HMC, i.e., if one has $\epsilon(n; \mathbf{k}) \approx \epsilon(n; \mathbf{k} + \mathbf{G})$ for all $\mathbf{G} \neq \mathbf{0}$, or whether the annihilation rate within the high-momentum regions is *deenhanced* or *overenhanced*, which means that we have

$$\epsilon(n; \mathbf{k} + \mathbf{G}) < \epsilon(n; \mathbf{k}) \quad \text{or} \quad \epsilon(n; \mathbf{k} + \mathbf{G}) > \epsilon(n; \mathbf{k}) \quad (42)$$

for $\mathbf{G} \neq \mathbf{0}$, respectively. Here we would like to emphasize that the above definitions of de- and overenhancement are not identical to the corresponding ones in recent papers by Kontrym-Sznajd and Rubaszek.³⁹ These authors speak about deenhancement and overenhancement if the inequalities $\epsilon(n; \mathbf{k} + \mathbf{G}) < \epsilon(n; \mathbf{k} + \mathbf{G}_{n\mathbf{k}})$ and $\epsilon(n; \mathbf{k} + \mathbf{G}) > \epsilon(n; \mathbf{k} + \mathbf{G}_{n\mathbf{k}})$, respectively, are fulfilled, where $\mathbf{G}_{n\mathbf{k}}$ represents the reciprocal-lattice vector belonging to the ‘‘main component’’ of the MDAP for the electron state $|n\mathbf{k}\rangle$. Despite the fact that this definition is more relevant from a physical point of view, for this paper, we prefer the definition (42) because it is more appropriate for the interpretation of our MDAP curves.

In order to investigate the question of de- or overenhancement from the point of view of lattice effects, we also calculated BML and LDA enhancement factors in Al, Cu, Pd and Mn for the nearest [(111), (110)] umklapp regions. Some results of this investigation are presented in Figs. 5 and 11–13.

In Fig. 5 we show BML and LDA enhancement curves for the first valence band of Al along the [111] direction both for the central and the nearest umklapp region. It is interesting to see that for momenta within the (111) umklapp region (i.e., along the points $L \rightarrow \Gamma' \rightarrow L'$), there appear considerable quantitative differences between the LDA and BML enhancement factors that are almost completely due to lattice effects on the e - p scattering, whereas the effects on the polarization play only a subordinate role. Concerning the momentum dependence of the enhancement factor in the [111] umklapp region, the BML and LDA results are qualitatively

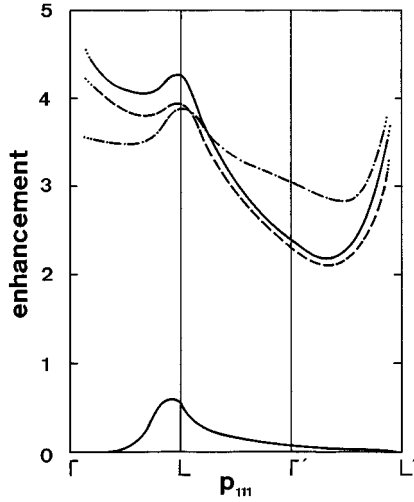


FIG. 11. State-dependent enhancement ϵ of the second band in fcc copper as a function of the extended momentum \mathbf{p} along the [111] direction. Solid line, enhancement ϵ^{OBML} ; dashed line, BML enhancement $\epsilon^{\text{scatter}}$ including $N_{\text{eff}}^{\text{LDA}}$ according to Eqs. (39) and (40); dash-dotted line, enhancement ϵ^{LDA} . The exact meaning of ϵ^{OBML} , $\epsilon^{\text{scatter}}$, and ϵ^{LDA} is given in Sec. VIII C of this paper. Dots at the beginning or the end of enhancement curves indicate MDAP values too small for a reliable numerical determination of ϵ . The solid curve at the bottom of the figure means the MDAP according to the IPM.

similar, but with a stronger momentum dependence of the BML enhancement factors. Of particular interest is the overenhancement of the MDAP of Al in the whole (111) umklapp region, an effect that is predicted by both theories (stronger for the BML approximation, weaker for the LDA). This result which represents an overenhancement effect de-

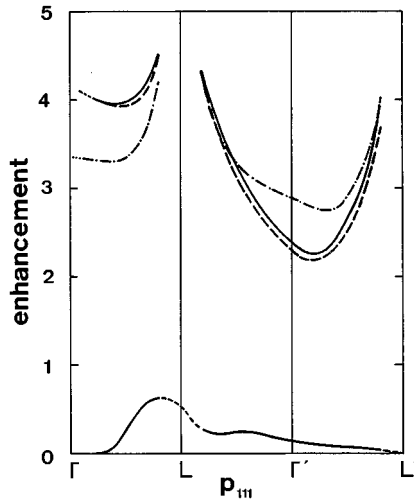


FIG. 12. State-dependent enhancement ϵ of the second band in fcc palladium as a function of the extended momentum \mathbf{p} along the [111] direction. Solid line, enhancement ϵ^{OBML} ; dashed line, BML enhancement $\epsilon^{\text{scatter}}$ including $N_{\text{eff}}^{\text{LDA}}$ according to Eqs. (39) and (40); dash-dotted line, enhancement ϵ^{LDA} . The exact meaning of ϵ^{OBML} , $\epsilon^{\text{scatter}}$, and ϵ^{LDA} is given in Sec. VIII C of this paper. The curve at the bottom of the figure means the MDAP according to the IPM, where the occupied (unoccupied) parts are given by solid (dashed) lines.

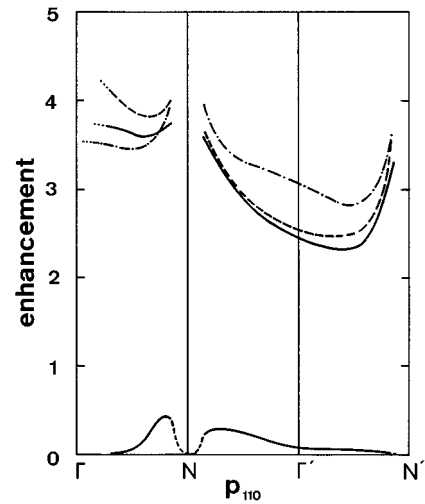


FIG. 13. State-dependent enhancement ϵ of the second band in bcc manganese as a function of the extended momentum \mathbf{p} along the [110] direction. The notations of this figure are the same as in Fig. 12.

tected by the BML method, contradicts a statement that can be frequently found in the literature (see Refs. 4, 24, and 39), namely, that the BML theory necessarily leads to a deenhancement of the annihilation rate in umklapp regions. Unfortunately, a quantitative experimental check of this theoretical prediction will hardly be possible because of the very small intensity of the annihilation rate belonging to the first valence band in Al in the umklapp regions (compare the IPM curve in Fig. 5).

More chances for an experimental check of BML or LDA enhancement results in the HMC are given in the umklapp regions of d -band metals such as Cu, Pd, and Mn, especially concerning the second valence bands of these metals along [111] or [110] due to the relatively high intensities of the corresponding MDAP (see the IPM curves in Figs. 11–13). At present, we are not able to give a detailed explanation of the HMC enhancement curves presented in these figures; all what we can say is the following. In the whole umklapp regions investigated [(111) for Cu and Pd, (110) for Mn], one observes a deenhancement of the partial annihilation rate, relatively moderate for the LDA results, but very significant for the BML results. These strong differences between LDA and the BML approximation are obviously mainly caused by lattice effects on the e - p scattering, whereas the effects on the polarization are comparatively unimportant indicated by the relatively small differences between the ϵ^{OBML} and $\epsilon^{\text{scatter}}$ curves.

In this connection, we think it is necessary to comment on the strong increase of the umklapp enhancement in the neighbourhood of the L' point for aluminum (Fig. 5) and copper (Fig. 11): in this region, the IPM curve has a zero point and, as a consequence, for a numerical evaluation of the corresponding enhancement, one has to divide very small enhanced rates by very small IPM rates. Due to unavoidable numerical uncertainties (compare the statements in Sec. VII C) of both numbers, large errors of the numerically ob-

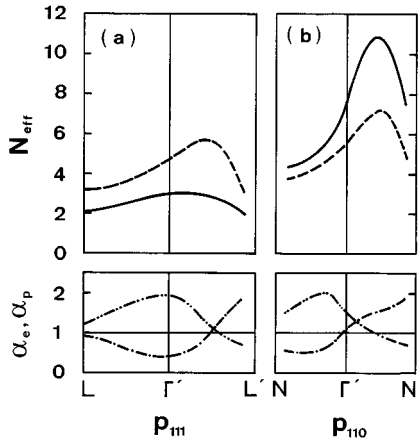


FIG. 14. Momentum-dependent optimized BML parameters N_{eff} , α_e , and α_p for the second bands of (a) copper and (b) manganese within the (111) and (110) umklapp region, respectively. Solid lines, $N_{\text{eff}}^{\text{BML}}$ (see Sec. VII A); dashed lines, $N_{\text{eff}}^{\text{LDA}}$ according to Eqs. (39) and (40); dash-dotted lines, α_e (see Sec. VII A). Dash-double-dotted lines, α_p (see Sec. VII A).

tained enhancement factors may appear. For this reason, we do not physically interpret our enhancement results in these very regions.

We shall now briefly discuss the behavior of the momentum-dependent BML parameters N_{eff} , α_e , and α_p within the (111) or (110) umklapp region for fcc or bcc metals, respectively. Concerning the parameters $N_{\text{eff}}^{\text{BML}}$ and $N_{\text{eff}}^{\text{LDA}}$, one observes, in general, the same relations between these parameters as for the central momentum region (see the discussion in Sec. VIII D 1): for metals with d bands lying below the Fermi energy (Cu and Pd), we have $N_{\text{eff}}^{\text{BML}} < N_{\text{eff}}^{\text{LDA}}$ within the whole umklapp region, whereas, for metals whose d bands lie both below and above E_F (Mn and V), one observes $N_{\text{eff}}^{\text{BML}} > N_{\text{eff}}^{\text{LDA}}$. However, in contrast to the relatively weak momentum dependence of N_{eff} within the central-momentum region (compare Table III), this quantity is strongly momentum dependent within the umklapp region, as is shown in Figs. 14(a) and 14(b) for copper and manganese. Due to correlations between the BML parameters, the marked momentum dependence of N_{eff} within the umklapp regions also leads to a relatively strong variation of the parameters α_e and α_p with the momentum vector \mathbf{p} , a behavior that can also be studied in Fig. 14.

In connection with these curves for copper and manganese, we would like to mention that the roughly symmetrical shape of these curves with respect to $\alpha = 1$ indicates a relatively strong correlation between α_e and α_p . Nevertheless, we found the minima of the LS optimization process of α_e and α_p usually very “sharp,” which means that the corresponding momentum-dependent parameters are numerically well defined, despite their mutual correlations. Additionally, a remark of Sec. VII A should be repeated here, namely, that the parameters α_e and α_p must not be interpreted as inverse values of effective electron and positron band masses, respectively, because of the fact that these parameters reflect not only the Bloch energies of the electron and positron scattering states but also the shapes of their wave functions and,

beyond that, the overlap of these Bloch functions and the shape of the Fermi surface.

E. Comparison of theoretical and experimental enhancement factors

Of course, neither enhancement factors of the electron-positron annihilation rate nor corresponding IPM rates are observable from a physical point of view. All that can be directly measured are fully integrated values of the momentum-dependent annihilation rate by the use of lifetime measurements or one- or two-dimensional rate distributions by 1D ACPAR, 2D ACPAR, or Doppler-broadening experiments. Therefore, a comparison of theoretical MDAP results with experimental data requires (aside from the use of relatively complicated 3D reconstruction methods⁷⁵) numerical integrations of the theoretical results with respect to one, two, or three momentum components. Such integrations are no great problem for the relatively simple LDA formalism, but, at least at present, extraordinarily time consuming for BML calculations, despite all efforts to accelerate our BML programs as much as possible.

For this reason, we had to use another way to confront our theoretical enhancement results with experiments. One possibility is to extract enhancement factors from experimental data, as proposed by Šob,^{8,9} who combined energy-dependent enhancement factors with l -dependent adjustable coefficients, which were optimized by a comparison with 1D ACPAR data. This method was successfully applied on FeAl and CuZn.^{12,13} Somewhat later, a similar technique of comparing theory and experiment was applied by the Geneva University Positron Group^{10,11,76} to vanadium, chromium, iron, and nickel and by Matsumoto and Wakoh^{14,15} to chromium and copper. These authors use a more flexible theoretical enhancement curve including more adjustable parameters than in the original work of Šob.

In the following, we refer to the summarizing work of Genoud⁷⁷ on e - p correlation effects in transition metals. This paper is based on theoretical MDAP values that were obtained by the linear muffin-tin orbital formalism including l -dependent enhancement factors as

$$\epsilon_l(\gamma) = a_{l0} + a_{l1}\gamma + a_{l2}\gamma^2 + (a_{l3}\gamma^3) \quad (43)$$

(the last term in parentheses is optional) with $\gamma = (E_{n\mathbf{k}} - E_{10}) / (E_F - E_{10})$ according to the semiempirical ansatz of Šob^{5,6} and of Mijnders and Singru.⁷ The quantities a_{li} , with $l = s, p, d, f, \dots$, are adjustable parameters that were determined by comparing the theoretical results with experimental 2D ACPAR data. Some of these parameters, given in Ref. 77 for Cu, Pd, and V are presented in Table V. By the use of these optimized parameters, the Geneva University Positron Group was able to extract band- and momentum-dependent enhancement factors from their experiments. Therefore, despite the fact that these enhancement factors were, of course, not directly measured, we shall call them, in the following, “experimental” enhancement factors ϵ^{expt} .

However, because of some risky aspects of this procedure (see Appendix B) and because of the lack of self-consistency in the theoretical approaches used for this investigation, it is

TABLE V. Parameters a_{li} for the s -, p -, and d -state enhancement according to Eq. (43) for copper, palladium, and vanadium as given in Ref. 77.

a_{li}	Cu	Pd	V
a_{s0}	1.0	1.0	1.0
a_{p0}	1.0	1.0	1.2
a_{d0}	0.9	0.85	1.0
a_{s1}	0.1	0.15	0.2
a_{p1}	0.1	0.15	0.1
a_{d1}	0.0	0.1	0.0
a_{s2}	0.0	0.0	0.0
a_{p2}	0.0	0.0	0.0
a_{d2}	-0.5	-0.3	0.0

clear that, at least for the present, a comparison of our LDA and BML enhancement results with ϵ^{expt} can only be qualitative and not quantitative. Nevertheless, as we shall demonstrate in the following, such a comparison gives valuable information about the physical relevance of the lattice effects investigated in this paper. Some results of this comparison for Cu, Pd, and V are presented in Figs. 15–17, where we show *relative* enhancement factors, i.e., factors normalized to the corresponding value of the first band at the Γ point along the [111] direction for Cu and Pd and (unlike the momentum direction for this metal in the previous subsections) along the [100] direction for V within the first BZ. The experimental enhancement curves according to Ref. 77 are given on the left-hand side (a) of these figures, and on the right-hand side (b), we present the corresponding theoretical curves obtained by the BML approximation (solid lines) and by the LDA (dash-dotted lines).

We start the discussion with copper (Fig. 15). Concerning the first band, the experimental curve shows a marked negative slope in the neighborhood of the boundary of the BZ, where this band is dominantly d -like. The shape of this enhancement curve is relatively well described by the corresponding BML curve, much better than by the LDA result. The experimental enhancement curve belonging to the second band decreases monotonically with increasing momentum, which is typical for a d band. The significant change of the (negative) slope close to the boundary of the BZ is due to the fact that the band becomes more and more sp -like in this momentum region. For small and medium momenta, the corresponding BML curve shows the same momentum dependence, but close to the boundary of the BZ, it reacts more sensitively upon the increasing sp character of the band, leading to a marked increase of ϵ^{OBML} , in contrast to the experimental curve. But despite this difference, it is obvious that the BML result describes the experimentally observed effects better than the LDA curve, which behaves almost purely Kahana-like. For palladium (Fig. 16), the situation is similar. One observes a principal agreement between the experimental and the theoretical enhancement curves with a significantly better performance of the BML approximation in comparison to the LDA.

At this point, it would be useful to include into the discussion also enhancement results obtained by the theory of Boron'ski and Jarlborg.⁵⁴ Until now, however, only few results yielded by this approach are available, for example,

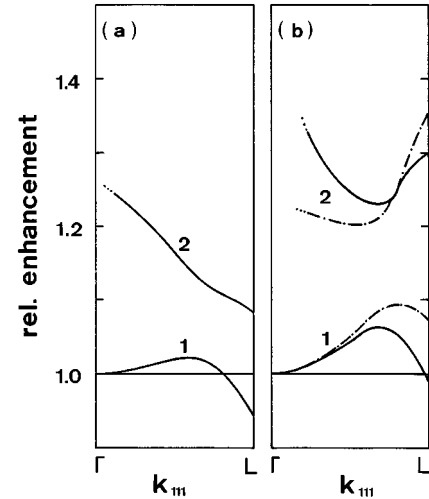


FIG. 15. State-dependent relative enhancement of the first and the second band (indicated by numbers 1 and 2) in fcc copper as a function of the reduced momentum \mathbf{k} along the [111] direction. (a) Experimental enhancement factors (Ref. 77) and (b) theoretical enhancement factors obtained by the OBML (solid lines) and by the LDA approach (dash-dotted lines). Dots at the beginning or the end of enhancement curves indicate MDAP values too small for a reliable numerical determination of ϵ .

momentum-dependent enhancement curves for Pd along the [110] direction (see Fig. 2 in Ref. 54). The most striking property of these enhancement curves in comparison to the BML and LDA results is their relatively weak momentum dependence, which seems to be in contradiction to the ϵ^{expt} values discussed in this section. On the other hand, there is some indication that the Boron'ski-Jarlborg (BJ) approach offers a better description of enhancement curves belonging to d states close to the Fermi surface than the BML approximation and the LDA. Anyway, for the future work on positron

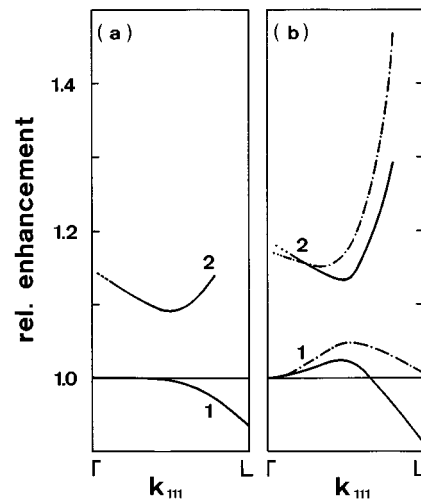


FIG. 16. State-dependent relative enhancement of the first and the second band (indicated by numbers 1 and 2) in fcc palladium as a function of the reduced momentum \mathbf{k} along the [111] direction. The notations of this figure are the same as in Fig. 15.

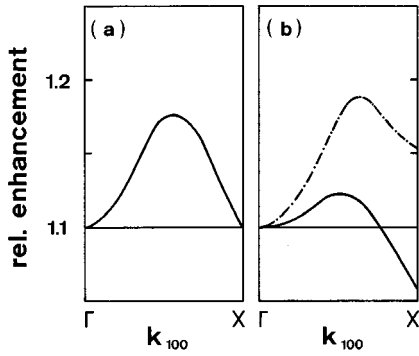


FIG. 17. State-dependent relative enhancement of the first band in bcc vanadium as a function of the reduced momentum \mathbf{k} along the [100] direction. The notations of this figure are the same as in Fig. 15.

annihilation in metals, a more extensive comparison of the BML approximation and the LDA with (BJ) enhancement results would be desirable.

Summarizing the information from Figs. 15 and 16, we can say that the inclusion of lattice effects in our OBML theory leads to improved qualitative agreement between theoretical and experimental enhancement factors. We can therefore conclude that the lattice effects described in this paper are of some importance for a proper theoretical description of positron annihilation in metals and should be taken into account.

However, at first sight, this conclusion seems to be too hasty if one observes Fig. 17, where we show experimental and theoretical results for the first band in vanadium along the ΓX line. In this case, it is evident that, in contrast to the two examples discussed before, the LDA enhancement curve corresponds better to the experimental curve than the BML result. This different behavior of V in comparison to Cu and Pd is also significant if one compares the optimized parameters a_{d2} for these metals according to Eq. (43) (see the last line in Table V). We think that the reason for this strange behavior is that we are confronted with the limits of the procedure of obtaining enhancement factors from the experiment, as proposed in Refs. 10, 11, 76, and 77 (compare Appendix B): namely, in the case of vanadium, the contribution of electron d states to the annihilation rate is much smaller than for Cu and Pd due to the fact that the second band in V contributing to the rate is mainly unoccupied (compare Fig. 4), with the consequence that the content of a d -enhanced annihilation rate in the experimental data is much smaller than in the other d metals discussed before. Consequently, one cannot expect a reliable fit for the $a_{d,i}$ enhancement parameters in the model function (43). Therefore, we suppose that the poor correspondence between the experimental curve and the BML curve for V is not caused by a bad performance of the BML theory but by exceeding the limits of the method of extracting enhancement results out of the 2D ACAR data. In fact, there is no reasonable argument that the first occupied valence band of vanadium should show completely different lattice effects of the enhancement than the first band of the other d -band metals investigated in this work.

IX. CONCLUSIONS

The main purpose of this paper is an investigation of the influence of lattice effects on the scattering between annihilating electrons and positrons. There are two different types of these lattice effects, namely, those that influence directly the interacting e - p pair and those that influence the polarization of the inhomogeneous electron gas and therefore the e - p interaction potential. The theoretical description of these lattice effects requires an inclusion of unoccupied electron and positron scattering states into the theory. This requirement is at least approximately fulfilled by our OBML theory, which is presented in this paper. As we extensively discussed in Sec. VII A, this theoretical approach can be reliably applied to metals with high and medium valence electron density (such as Al, Cu, and the transition metals), but only with some reservation to metals with lower electron density.

Within the first BZ, the lattice effect on the e - p scattering causes, for all metals and all occupied electron states investigated, a considerable increase of the enhancement factors in comparison with the corresponding LDA results: close to the Γ point, one observes an increase of about 6% for Al and between 10% and 23% for the d -band metals Cu, Pd, Mn, and V. Additionally, for bands with a more or less marked d character, the shape of the LDA enhancement curves is also changed by this lattice effect: if the d character dominates, one observes a negative momentum dependence of the enhancement that is significantly stronger than for the LDA results. On the other hand, if the band is dominantly sp -like, the positive (Kahana-like) momentum dependence of the corresponding LDA enhancement factors is reduced. This argumentation is also supported by a comparison of our results with enhancement factors extracted from 2D ACPAR experiments.⁷⁷

Very interesting is the role of the second effect called the ‘‘lattice effect on the polarization,’’ which does not drastically change the momentum dependence of the enhancement curves but considerably influences the magnitude of the enhancement: in fact, it shifts the enhancement curves to higher or lower values depending on the energetic position of the d bands with respect to the Fermi energy. This shift is negligible in the absence of d bands, as is the case for Al. For the d -band metals Cu and Pd, we observe a moderate and small positive shift of the enhancement curves, respectively. On the contrary, Mn shows a moderate and V a strong negative shift, i.e., to smaller values of the enhancement, which leads to a more or less marked cancellation of the lattice effect on the e - p scattering. For the second band of vanadium, the lattice effect of the polarization even overcompensates the lattice effect on the e - p scattering, with the consequence that, in this case, the enhancement according to our OBML theory is smaller than the corresponding LDA result.

In this paper, we also present a comparison of BML and LDA enhancement factors in simple and d -band metals for high-momentum components of the MDAP. In general, the BML and LDA results are comparable from a qualitative point of view. Quantitatively, however, the momentum dependence of the enhancement is more marked for the BML than for the LDA enhancement curves. This can be observed for Al, where both theoretical methods show an overenhancement within the (111) umklapp region, but also for the

d -band metals Cu, Pd, and Mn, where we observed a moderate enhancement for the LDA results and a strong enhancement for the BML results. These differences between BML and LDA are mainly due to the lattice effect on the e - p scattering, whereas the lattice effect on the polarization is less important.

Summarizing our results, we can say that, for a proper theoretical description of the electron-positron annihilation process both in simple and in d -band metals and both for the central momentum region and the umklapp regions, the influence of the crystal lattice is significant and should not be neglected.

ACKNOWLEDGMENTS

The author thanks Dr. P. Genoud for sending him his enhancement results prior to publication. He is also indebted to many colleagues, especially from the group of Professor H. Stachowiak from the Polish Academy of Sciences in Wroclaw and from the group of Professor M. Peter of the University of Geneva, for many interesting and helpful discussions about the electron-positron interaction in metals. His special thanks are due to Dr. M. Šob for valuable suggestions and for his continuing interest in this work and to the Fonds zur Förderung der Wissenschaftlichen Forschung of Austria for its financial support under Project No. P09265-TEC.

APPENDIX A

It is clear that the use of the RPA for the e - p interaction potential has the consequence that our BML and LDA results are not self-consistent with respect to V^{ep} , a fact that makes a direct comparison of our results with experimental annihilation rates more difficult. However, concerning the sensitivity of the MDAP and enhancement factors on different e - p interaction potentials, we learn from a comparison of RPA potentials with fully self-consistent potentials for the homogeneous electron gas³ that this sensitivity is very strong in the medium and low electron density region for, say, for $r_s > 3$ a.u., but is moderate for smaller values of the electron density parameter, which means, in the region of r_s , which is especially interesting for our calculations (compare the discussion in Sec. VII A). Therefore, if we use this result for the inhomogeneous electron gases of the metals that we study in this paper, we expect that the application of more elaborate e - p potentials than the RPA would not significantly change the results and the physical conclusions of our work.

A second point concerns the use of a *static* approximation to the dynamical e - p interaction potential. For the homogeneous electron gas, this simplification of the theory is justified by earlier results of Carbotte and Kahana,⁶¹ who pointed out that dynamical corrections to the annihilation rate due to the e - p interaction potential are largely compensated by dynamical corrections due to electron and positron self-energy terms. In his work on positron annihilation in real metals,⁴⁷ Carbotte repeats the arguments of Ref. 61 without discussing any new aspects that might occur from the inhomogeneity of

the electron gas. For the present paper, we take over Carbotte's argumentation in the following way: as we extensively pointed out in Sec. II, the electron and positron Green's functions used in the BML approximation are based on the Schrödinger-like equations (6) and (7). In these equations, the effects of interactions of a single particle with the other electrons in the crystal are included by single-particle Hartree and exchange-correlation potentials. We can say that these potentials have approximately the same effect on the electron and positron propagators as the inclusion of Hartree-Fock and *static* correlation self-energy insertions into these propagators. According to Carbotte, the use of a dynamical e - p interaction potential V^{ep} in our BML formulas would also require the inclusion of the dynamical part of these self-energy insertions into the single-particle Green's functions (4) and (5) which would be an extremely complicated task. For this reason, until now, there have been no investigations on the question whether the cancellation of the dynamical parts of electron and positron self-energy terms and V^{ep} in the ladder diagrams is as effective for the inhomogeneous electron gas as for the homogeneous one.

Nevertheless, special studies on both topics discussed in this appendix, namely, concerning (i) the use of e - p potentials beyond the RPA, eventually by an inclusion of exchange-correlation field corrections to the V^{ep} matrix, and (ii) the role of dynamical corrections to these potentials in theoretical MDAP calculations for real metals would be highly desirable; the present author plans efforts in both directions for the future.

APPENDIX B

The procedure of extracting band- and momentum-dependent enhancement factors from 2D ACPAR experiments, as proposed by the Geneva University Positron Group^{10,11,76,77} is without any doubt of great importance for comparisons between theoretical and experimental enhancement results. Nevertheless, one should be aware that this procedure (described in Sec. VIII E) includes some risks.

At first, one might be concerned that the simple analytical form of the enhancement model Eq. (43) might be inappropriate for the given problem. We do not think so because the model includes enough parameters to offer sufficient flexibility. However, for several reasons,¹⁰ the a_{li} coefficients published in Refs. 10, 11, 76, and 77 do not follow from a LS comparison of theory and experiment, but reflect the best agreement of the theoretical and experimental data for a relatively small number of trials. So, for example, many of the a_{s0} and a_{p0} parameters are simply set to one, which might not always be the best choice. Another problematic point is due to the fact that the model parameters a_{li} are the same for both the LMC and the HMC regions, which means that these parameters only reflect average values for the whole momentum space. This might be risky especially for transition metals where the d -band enhancement is quite different for LMC and HMC regions. A third point that should be kept in mind is that some parameters in Eq. (43) might be unreliably determined because of too small a content of the MDAP with respect to these parameters, an objection that has already been mentioned in Ref. 10 and is discussed for the example vanadium in Sec. VIII E of the present paper.

- ¹S. Kahana, Phys. Rev. **129**, 1622 (1963).
- ²E. Boroński, Z. Szotek, and H. Stachowiak, Phys. Rev. B **23**, 1785 (1981).
- ³A. Rubaszek and H. Stachowiak, Phys. Rev. B **38**, 3846 (1988).
- ⁴H. Stachowiak and A. Rubaszek, Solid State Phenom. **28 & 29**, 7 (1993).
- ⁵M. Šob, in *Proceedings of the 8th Annual International Symposium on the Electronic Structure of Metals and Alloys*, edited by P. Ziesche (Technische Universität Dresden, Dresden, 1978), p. 170.
- ⁶M. Šob, in *Positron Annihilation*, edited by R. R. Hasiguti and K. Fujiwara (The Japanese Institute of Metals, Sendai, 1979), p. 309.
- ⁷P. E. Mijnarends and R. M. Singru, Phys. Rev. B **19**, 6038 (1979).
- ⁸M. Šob, in *Proceedings of the 10th Annual International Symposium on the Electronic Structure of Metals and Alloys*, edited by P. Ziesche (Dresdener Seminar für Theoretische Physik, Dresden, 1980), p. 106.
- ⁹M. Šob, J. Phys. F **12**, 571 (1982).
- ¹⁰A. K. Singh, A. A. Manuel, T. Jarlborg, Y. Mathys, E. Walker, and M. Peter, Helv. Phys. Acta **59**, 410 (1986).
- ¹¹P. Genoud, A. K. Singh, A. A. Manuel, T. Jarlborg, E. Walker, M. Peter, and M. Weller, J. Phys. F **18**, 1933 (1988).
- ¹²J. Svoboda and M. Šob, Philos. Mag. B **48**, 523 (1983).
- ¹³M. Šob, J. Svoboda, W. Gerber, O. Brümmer, and G. Dlubek, in *Proceedings of the 13th Annual International Symposium on the Electronic Structure of Metals and Alloys*, edited by P. Ziesche (Dresdener Seminar für Theoretische Physik, Dresden, 1983), p. 28.
- ¹⁴M. Matsumoto and S. Wakoh, J. Phys. Soc. Jpn. **56**, 3566 (1987).
- ¹⁵M. Matsumoto and S. Wakoh, Physica B **149**, 57 (1988).
- ¹⁶E. Bonderup, J. U. Andersen, and D. N. Lowy, Phys. Rev. B **20**, 883 (1979).
- ¹⁷B. Chakraborty, Phys. Rev. B **24**, 7423 (1981).
- ¹⁸S. Daniuk, G. Kontrym-Sznajd, J. Mayers, A. Rubaszek, H. Stachowiak, P. A. Walters, and R. N. West, in *Positron Annihilation*, edited by P. C. Jain, R. M. Singru, and K. P. Gopinathan (World Scientific, Singapore, 1985), pp. 43 and 279.
- ¹⁹S. Daniuk, G. Kontrym-Sznajd, A. Rubaszek, H. Stachowiak, J. Mayers, P. A. Walters, and R. N. West, J. Phys. F **17**, 1365 (1987).
- ²⁰T. Jarlborg and A. K. Singh, Phys. Rev. B **36**, 4660 (1987).
- ²¹M. Šob, Mater. Sci. Forum **175–178**, 855 (1995).
- ²²G. Kontrym-Sznajd and J. Majsnerowski, Solid State Commun. **70**, 593 (1989).
- ²³S. Daniuk, G. Kontrym-Sznajd, J. Majsnerowski, M. Šob, and H. Stachowiak, J. Phys. Condens. Matter **1**, 6321 (1989).
- ²⁴G. Kontrym-Sznajd and J. Majsnerowski, J. Phys. Condens. Matter **2**, 9927 (1990).
- ²⁵G. Kontrym-Sznajd, Mater. Sci. Forum **105–110**, 691 (1992).
- ²⁶S. Daniuk, J. Phys. Condens. Matter **1**, 5561 (1989).
- ²⁷G. Kontrym-Sznajd and J. Majsnerowski, Mater. Sci. Forum **105–110**, 699 (1992).
- ²⁸G. Kontrym-Sznajd and M. Šob, J. Phys. F **18**, 1317 (1988).
- ²⁹T. Jarlborg, B. Barbiellini, E. Boroński, P. Genoud, and M. Peter, J. Phys. Chem. Solids **52**, 1515 (1991).
- ³⁰A. A. Manuel, B. Barbiellini, M. Gauthier, L. Hoffmann, T. Jarlborg, S. Massidda, M. Peter, W. Sadowski, A. Shukla, and E. Walker, J. Phys. Chem. Solids **54**, 1223 (1993).
- ³¹B. Barbiellini, M. Gauthier, L. Hoffmann, T. Jarlborg, A. A. Manuel, S. Massidda, M. Peter, and G. Triscone, Physica C **229**, 113 (1994).
- ³²K. O. Jensen, J. Phys. Condens. Matter **1**, 10 595 (1989).
- ³³S. Daniuk, M. Šob, and A. Rubaszek, Phys. Rev. B **43**, 2580 (1991).
- ³⁴M. J. Puska, J. Phys. Condens. Matter **3**, 3455 (1991).
- ³⁵P. A. Sterne and J. H. Kaiser, Phys. Rev. B **43**, 13 892 (1991).
- ³⁶B. Barbiellini, P. Genoud, and T. Jarlborg, J. Phys. Condens. Matter **3**, 7631 (1991).
- ³⁷B. Barbiellini, M. J. Puska, T. Torsti, and R. M. Nieminen, Phys. Rev. B **51**, 7341 (1995).
- ³⁸M. Šob, S. Daniuk, and A. Rubaszek, Mater. Sci. Forum **105–110**, 861 (1992).
- ³⁹G. Kontrym-Sznajd and A. Rubaszek, Phys. Rev. B **47**, 6950 (1993); **47**, 6960 (1993).
- ⁴⁰K. Fujiwara, T. Hyodo, and J. Ohya, J. Phys. Soc. Jpn. **33**, 1047 (1972).
- ⁴¹B. B. J. Hede and J. P. Carbotte, J. Phys. Chem. Solids **33**, 727 (1972).
- ⁴²H. Sormann, P. Nowak, P. Kindl, and W. Puff, in *Positron Annihilation*, edited by P. G. Coleman, S. C. Sharma, and L. M. Diana (North-Holland, Amsterdam, 1982), p. 218.
- ⁴³H. Sormann and W. Puff, in *Positron Annihilation* (Ref. 18), p. 161.
- ⁴⁴M. Šob, Solid State Commun. **53**, 249 (1985).
- ⁴⁵M. Šob, J. Phys. F **15**, 1685 (1985).
- ⁴⁶M. Šob, in *Positron Annihilation*, edited by L. Dorikens-Vanpraet, M. Dorikens, and D. Segers (World Scientific, Singapore, 1989), p. 131.
- ⁴⁷J. P. Carbotte, Phys. Rev. **144**, 309 (1966).
- ⁴⁸J. P. Carbotte and A. Salvadori, Phys. Rev. **162**, 290 (1967).
- ⁴⁹An extensive derivation of the BML formulas quoted in Sec. IV of this paper from first principles is given by D. Wallner, Ph.D. thesis, Technical University of Graz, 1995 (unpublished).
- ⁵⁰H. Sormann (unpublished).
- ⁵¹L. Oberli, A. A. Manuel, R. Sachot, P. Descouts, M. Peter, L. P. L. M. Rabou, P. E. Mijnarends, T. Hyodo, and A. T. Stewart, Phys. Rev. B **31**, 1147 (1985).
- ⁵²H. Sormann, Phys. Status Solidi B **142**, K45 (1987).
- ⁵³H. Sormann, in *Positron Annihilation* (Ref. 46) p. 272.
- ⁵⁴E. Boroński and T. Jarlborg, Mater. Sci. Forum **105–110**, 607 (1992).
- ⁵⁵E. Boroński, Mater. Sci. Forum **105–110**, 181 (1992).
- ⁵⁶E. Boroński, S. Daniuk, and H. Stachowiak, Acta Phys. Polon. A **83**, 255 (1993).
- ⁵⁷H. Sormann and D. Wallner, Mater. Sci. Forum **105–110**, 845 (1992).
- ⁵⁸H. Sormann, Acta Phys. Polon. A **83**, 381 (1993).
- ⁵⁹H. Sormann and D. Wallner, Mater. Sci. Forum **175–178**, 863 (1995).
- ⁶⁰H. Sormann and D. Wallner, Acta Phys. Polon. A **88**, 225 (1995).
- ⁶¹J. P. Carbotte and S. Kahana, Phys. Rev. **139**, A213 (1965).
- ⁶²J. P. Carbotte, Phys. Rev. **155**, 197 (1967).
- ⁶³E. Boroński and R. M. Nieminen, Phys. Rev. B **34**, 3820 (1986).
- ⁶⁴A. Rubaszek (private communication).
- ⁶⁵H. Stachowiak, Mater. Sci. Forum **175–178**, 209 (1995).
- ⁶⁶S. L. Adler, Phys. Rev. **126**, 412 (1962); N. Wiser, *ibid.* **129**, 62 (1963).
- ⁶⁷A. Fleszar and R. Resta, Phys. Rev. B **31**, 5305 (1985).

- ⁶⁸M. S. Hybertsen and S. G. Louie, *Phys. Rev. B* **35**, 5585 (1987); **35**, 5602 (1987).
- ⁶⁹A. L. Fetter and J. D. Walecka, *Quantum Theory of Many-Particle Systems* (McGraw-Hill, New York, 1971), p. 158.
- ⁷⁰L. Hedin and B. I. Lundqvist, *J. Phys. C* **4**, 2064 (1971).
- ⁷¹G. Gilat and L. J. Raubenheimer, *Phys. Rev.* **144**, 390 (1966).
- ⁷²W. Jones and N. H. March, *Theoretical Solid State Physics* (Wiley, London, 1973), Vol. 1, p. 76ff.
- ⁷³A. Rubaszek and H. Stachowiak, *Phys. Status Solidi B* **124**, 159 (1984).
- ⁷⁴See, e.g., D. A. Papaconstantopoulos, *Handbook of the Band Structure of Elemental Solids* (Plenum, New York, 1986).
- ⁷⁵See, e.g., G. Kontrym-Sznajd, *Phys. Status Solidi A* **117**, 227 (1990), and references therein.
- ⁷⁶A. A. Manuel, A. K. Singh, T. Jarlborg, P. Genoud, L. Hoffmann, and M. Peter, in *Positron Annihilation* (Ref. 46), p. 109.
- ⁷⁷P. Genoud, Ph.D. thesis, Université de Genève, 1990 (unpublished).